TRIBHUVAN UNIVERSITY
INSTITUTE OF ENGINEERING
PULCHOWK CAMPUS

BREAST CANCER DETECTION USING MICRO STRIP PATCH ANTENNA

By:
Brajesh Yadav (077BME015)
Rabin Jung Kuwar (077BME026)
Ram Raj Bajracharya (077BME029)
Saurav Kafle (077BME038)

A PROJECT REPORT
SUBMITTED TO THE DEPARTMENT OF MECHANICAL AND AEROSPACE ENGINEERING IN PARTIAL FULFILLMENT OF THE REQUIREMENT FOR THE DEGREE OF BACHELOR IN MECHANICAL ENGINEERING

DEPARTMENT OF MECHANICAL AND AEROSPACE ENGINEERING
LALITPUR, NEPAL

March 2025

COPYRIGHT PAGE

TRIBHUVAN UNIVERSITY
INSTITUTE OF ENGINEERING, PULCHOWK CAMPUS
DEPARTMENT OF MECHANICAL AND AEROSPACE ENGINEERING

The undersigned certify that they have read, and recommended to the Institute of Engineering for acceptance, a project report entitled **"BREAST CANCER DETECTION USING MICROSTRIP PATCH ANTENNA"** submitted by Brajesh Yadav, Rabin Jung Kunwar, Ram Raj Bajracharya, and Saurav Kafle in partial fulfillment of the requirements for the degree of Bachelor of Mechanical Engineering.

Supervisor, Dr. Ajay Kumar Jha
Associate Professor
Department of Mechanical and Aerospace Engineering
IOE, Pulchowk Campus

External Examiner, Er. Rajiv Jha
Biomedical Engineer
Cancer Hospital Nepal

Tribhuvan University
Institute of Engineering
Department of Mechanical and Aerospace Engineering
Pulchowk Campus

Committee Chairperson, Dr. Sudip Bhattrai
Assistant Professor
Head, Department of Mechanical and Aerospace Engineering
IOE, Pulchowk Campus

Date: 2025/05/04

ABSTRACT

A microwave imaging system employing a 2.4 GHz microstrip patch antenna (**FR4** substrate dimensions: 76×58 mm, patch: 38×29 mm) was designed and validated for non-invasive breast cancer detection. The antenna was modeled in **CST Microwave Studio**, fabricated via etching, and tested using a two-port **NanoVNA**. A multi-layered breast phantom, comprising 3D-printed skin, adipose, glandular tissue, and tumor inclusions ($\varepsilon_r = 50.9, \sigma = 4\,\mathrm{S/m}$) was developed to simulate dielectric contrast. Scattering parameters (S_{11}, S_{21}) were analyzed, with resonance observed at 2.4 GHz (-27 dB return loss) in simulation and 2.55 GHz (-25.06 dB) experimentally. Tumor images were reconstructed using the **Delay-and-Sum (DAS)** algorithm based on MERITS [1] in **MATLAB**.

Specific Absorption Rate (SAR) analysis confirmed compliance with safety standards, yielding 0.683 W/kg averaged over 10 g of tissue, which is approximately 65% below the **ICNIRP[2]/IEEE[3]** limit (2 W/kg) and less than 50% of the **FCC[4]** threshold for 1 g (1.6 W/kg). Challenges such as hardware limitations (e.g., the two-antenna NanoVNA setup) and environmental noise impacted the experimental resolution. Nevertheless, the study validated microwave imaging as a radiation-free diagnostic tool, with future recommendations including biomimetic phantoms, multi-antenna arrays, and advanced signal processing algorithms to enhance clinical applicability.

Keywords: Breast Cancer, Microstrip Antenna, SAR Compliance, DAS Algorithm, CST.

ACKNOWLEDGMENT

We would like to sincerely thank the Department of Mechanical and Aerospace Engineering, IOE, Pulchowk Campus, Lalitpur, for giving us the opportunity to work on this project, which has helped us apply and improve the knowledge and skills we have gained during our Bachelor of Mechanical Engineering studies. We are also grateful to our supervisor, Assoc. Prof. Dr. Ajay Kumar Jha, for his constant support and guidance throughout the project.We also extend our sincere thanks to our external supervisor, Er. Ravi Jha, for his valuable suggestions and guidance for completion of this project.

We would also like to thank Orion Space for providing the necessary environment for testing and experiments, and Digitronix Nepal for their valuable help and guidance during the antenna fabrication process. Finally, we would also like to convey our thanks to the teachers, seniors, juniors, and our friends who have helped us in any way in completion of this project.

Sincerely,

Brajesh Yadav (077BME015)

Rabin Jung Kuwar (077BME026)

Ram Raj Bajracharya (077BME029)

Saurav Kafle (077BME038)

TABLE OF CONTENTS

LIST OF FIGURES

LIST OF TABLES

LIST OF ABBREVIATIONS

DAS Delay And Sum Algorithm

DMAS Delay Multiply And Sum Algorithm

BPF Band Pass Filter

ADC Analog To Digital Converter

SAR Specific Absorption Rate

LPF Low Pass Filter

TGC Time Gain Compensation

VNA Vector Network Analyzer

DUT Device Under Test

CDAS Coherence Delay and Sum

CHAPTER 1:
INTRODUCTION

1.1 Background

Cancer is a disease caused due to abnormal growth of cells at a rapid rate. Therefore, it is considered as the most deadliest diseases if not treated within its first and second stages. But detection of these abnormal cells at early stage has always been a difficult task. The detection of cancer at last stages has been the crucial reason for the death of individuals. Among all the types of cancers discovered till today, breast cancer is the most common type diagnosed to about 7.8 million women globally in the past 5 years[6]. While it is imperative to address this situation and to find a solution by developing a cure, it is even more important to develop methods to detect its presence in the body. Early diagnosis of breast cancer includes imaging methods which are X-ray, Mammography, Ultrasound (US), and Magnetic Resonance Imaging (MRI). While existing methods give good result, there have been serious deficiencies. Although Mammography is the best method of breast imaging, this method can give results of false negative rates[7]. X-Ray Mammography, has been the standard clinical technique for detecting breast abnormalities and women are encouraged to participate in breast cancer screening programs involving regular mammograms[8], however, increased levels of fibro-glandular tissue in high density breasts may obscure the overall sensitivity of mammography. According to reports from X-Ray mammography examinations conducted by the US Medical Institution, the limitations of mammography include missing 15% of breast cancers with false negative rates ranging from 4 to 34%[9]. The diagnosis of suspected lesions on mammograms often involves more imaging or waiting for a biopsy. These tools have been one an only option for the diagnosis of cancerous cells, however, scientists and researchers have taken keen interest in using micro wave technology and radio frequency for improving the sensitivity (ability to correctly identify those with tumors) and specificity (ability to correctly identify those without tumors) of existing imaging systems.

X-rays imaging works by passing a controlled amount of radiation through the body, which is then captured on a detector. Different tissues absorb amounts of X-rays, producing an image that can reveal abnormalities in tumors. Alternatively, ultrasound

imaging is another option. Adler et al.[10] used Doppler ultrasound color flow imaging in the study of breast cancer. Abnormalities, masses, architectural distortions, mass shapes, mass margins, and so many other characteristics of breast cancer were observable using this method. Although ultrasound is the option that offers high spatial resolution, and breast tumor angiogenesis is trackable using Doppler flow imaging, image contrast is poor in this approach because normal and cancerous tissues each show almost similar acoustical responses to stimuli since both are soft tissue types[11].
More recently, another way of tracking is microwave imaging, which shows good levels of relevancy to diagnose breast cancer in male and female patients. Meany et al. [12]developed a microwave tomography system for experimental breast imaging. Basically, microwave imaging relies on density-based interactions in which dielectric-based inter actions are used to detect breast cancer in its early stages. In this approach, dielectric properties of tissues, such as relative permittivity and conductivity, are effective.
This imaging scenario, however, provides poor spatial resolution in biological tissues sampling; the reason for this poor resolution is related to the long wavelength of microwaves. On contrary, microwaves do not require ionization of tissues which seems to be ideal for imaging and signal processing process. In this report we generate microwave signal at 2.4 GHz through micro-patch antenna. It can simply be generalized as a monopole antenna mounted on a ground plane. Because of the ground plane, patch antenna has more bandwidth as compared to the monopole antenna which seems to be favorable for this experiment.

1.2 Problem Statement

There's always questions about radiation exposure from medical imaging. Individuals want to know if radiation from mammograms, bone density tests, computed tomography (CT) scans, and so forth will increase their risk of developing cancer. For most women, there's very little risk from routine x-ray imaging such as mammography or dental x-rays. But many experts are concerned about an explosion in the use of higher radiation–dose tests, such as CT and nuclear imaging. Cancer being one of the most fatal disease in this globe, it becomes much more difficult when we come to know that,

these cancer detecting tools are increasing the growth of cancerous cell in our body.

Over 80 million CT scans are performed in the United States each year, compared with just three million in 1980. There are good reasons for this trend. CT scanning and nuclear imaging have revolutionized diagnosis and treatment, almost eliminating the need for once-common exploratory surgeries and many other invasive and potentially risky procedures. The radiation you get from x-ray, CT, and nuclear imaging is ionizing radiation — high-energy wavelengths or particles that penetrate tissue to reveal the body's internal organs and structures. Ionizing radiation can damage DNA, and although your cells repair most of the damage, they sometimes do the job imperfectly, leaving small areas of disrepair. The result is DNA mutations that may contribute to cancer years down the road.

Exposure to ionizing radiation from natural or background sources hasn't changed since about 1980, but Americans' total per capita radiation exposure has nearly doubled, and experts believe the main reason is increased use of medical imaging. The proportion of total radiation exposure that comes from medical sources has grown from 15% in the early 1980s to 50% today. CT alone accounts for 24% of all radiation exposure in the United States, according to a report issued in March 2009 by the National Council on Radiation Protection and Measurements[13]. MRI is strictly prohibited to patients with implanted pacemakers, Cochlear implants, Neurostimulators, Bone-growth stimulators, and Certain intrauterine contraceptive devices. Due to the potential for a harmful increase in the temperature of the amniotic fluid, MRI is not advised for pregnant patients[14].

Thus, we proposed the development and implementation of micro patch antenna system designed specifically to detect breast cancer. The core problem can be articulated as follows:

How can we develop a non invasive, cost effective, sensitive, specific and accurate breast cancer detection system using micro patch antenna, What are the practical challenges associated with its development, and How can we make this system familiar among medical scholars?

1.3 Objectives

1.3.1 Main Objective

To design and fabricate non invasive, cost effective, sensitive, specific and accurate breast cancer detection system using Microwave technology.

1.3.2 Specific Objectives

- To design a micro patch antenna optimized for detecting differences in the dielectric properties of healthy and cancerous breast tissues.
- To conduct rigorous testing using breast phantoms (artificial models of breast tissue) with embedded tumors of various sizes and dielectric properties in CST studio software.
- To select bio compatible materials that ensure patient safety and comfort while maintaining optimal antenna performance.
- To ensure that the obtained SAR values fall within the safe and non-harmful range.
- To develop and implement advanced signal processing algorithms to accurately interpret the signals received from the antenna.

1.4 Scope and Limitations

1.4.1 Scope

- It can be safer and cheaper alternative to X-ray mammography, CT scans and nuclear imaging.
- The development of accurate detection system can lead to disruption in bio medical technology.

1.4.2 Limitations

- The limitation of this method is designing a proper antenna. It involves overcoming challenges related to size, impedance matching, low-power requirements, bio-compatibility, and the complex biological environment of the body.
- In present context, source of antenna has been serious problem for efficient conduction of the experiment. We have access to only 2 port Nano-VNA . This has limited us to use only two antennas resulting in poor image resolution.
- Developing a human tissue-mimicking phantom is limited by technical challenges like dielectric accuracy, stability, and reproducibility, alongside high material and fabrication costs.

1.5 System Used (For Development/ Implementation)

1.5.1 Hardware used

The major hardware that are used in our project are:

- Double Side Copper plate
- Substrate(Epoxy or Polycarbonate)
- SMA connector
- NanoVNA
- Copper wire(For feeding)
- ADC
- Coaxial Cable
- Amplifier

1.5.2 Software Used

The major software that are used in our project are:

- CST
- HFSS
- Python
- Matlab
- SolidWorks
- COMSOL
- NanoVNA 0.6.2

CHAPTER 2:
LITERATURE REVIEW

2.1 Microwave Scattering Properties of Malignant and Normal Breast Tissues

The detection of breast cancer using microwave signals is based on the differences in the scattering properties of malignant and normal breast tissues. These differences arise primarily due to the varying water content in the tissues. Malignant tumors generally have a higher water content, which results in a larger scattering cross-section compared to normal fatty tissues. This property allows microwave-based imaging techniques to detect tumors by analyzing the microwave signal interactions with breast tissues.

Yiou Cheng and Minghuan Fu took samples of freshly excised breast tissues (n=509) from 98 patients that were identified as normal, benign tumor, or malignant cancer via histology. Further samples were prepared and the microwave effective dielectric permittivity and effective conductivity were measured every 0.0375 GHz from 0.5 to 8 GHz. These parameters were compared among the breast tissues types. They found that the effective relative permittivity and effective conductivity at each frequency was significantly higher than in normal breast tissue. The standard deviation of each parameter was narrowest at 2.5GHz in both normal and malignant breast tissues. This result made them conclude that the effective permittivity and effective conductivity, measured via microwave technology, could differentiate breast cancer from normal and malignant tissues. Their research gave us insight for the values of dielectric properties of different types of breast tissues at different frequencies. [15]

Hagness et al. [16] demonstrated that malignant tumors, which possess higher water content, exhibit significantly larger microwave scattering cross-sections than normal breast tissues, which are mainly composed of fat and have a lower water content. This difference in microwave scattering behavior is critical for non-invasive breast cancer detection methods. The dielectric properties of tissues, including the relative permittivity (ε_r) and electrical conductivity (σ), differ considerably between normal and malignant breast tissues. Gabriel et al. [17] reported that normal breast tissues have a relative permittivity of around $\varepsilon_r = 9$ and a conductivity $\sigma = 0.4$ S/m. In contrast, malignant tumors exhibit much higher values, with $\varepsilon_r = 50$ and $\sigma = 4$ S/m. This increase in permittivity and conductivity is attributed to the tumor's higher water content, which

significantly influences the propagation of microwave signals in the tissues.

2.2 Microwave Breast Cancer Detection Approaches

Researchers and scientists have grown their interest in bringing an alternative to X-ray mammography, CT scans, nuclear treatment to reduce exposure of radiation in human body. They needed a wave which was less radioactive but carried enough energy for the propagation of signal. The wave compatible for this was microwave having frequency range from 300 MHz to 300 GHz. This range of frequency are more effective and beneficial for biomedical applications, exclusively for biomedical imaging and therapy. The main point of Microwave breast imaging is the electrical properties differences such as permittivity and conductivity. Tumor tissues have higher values than healthy tissues in terms of these electrical properties.

Numerous studies on microwave breast cancer detection systems have primarily relied on simulations and phantom scans, which are synthetic models of human tissue. Despite these efforts, the true effectiveness of any biomedical device is ultimately determined by clinical outcomes. To date, only a limited number of research groups have published clinical trial results for these systems.

One notable system operates within the frequency range of 0.5 GHz to 2.9 GHz and employs sixteen monopole antenna arrays. These antennas are connected to a 16-channel switching matrix and a digital radio frequency generator. The system is divided into two sub-arrays, each containing eight antennas. Each antenna transmits electromagnetic signals sequentially to the other 15 antennas, resulting in a total of 240 data points collected at each frequency [12].

Another research initiative has developed two distinct microwave systems for breast cancer detection. The first system is a clinically validated device registered with Health Canada, utilizing a rotating bi static radar configuration. The second system is a portable breast cancer detection unit, which has not yet undergone clinical validation [18, 19].

The portable detection system has one transmitter and 13 receivers. They're set up in a semi-circle with 4 mm between each receiver to avoid signal overlap and capture as much information as possible. It operates between 1.5 GHz and 6 GHz, sending out signals. To ensure accuracy, adjustments are made using numbers obtained from computer

simulations. However, sometimes what we see in simulations doesn't match with real experiment. The differences observed up to -4% to 3% in wide-open areas and up to $\pm$15% in different situations. The system detects changes in the electromagnetic field caused by scattering objects by converting the received RF signals to DC voltage. The power levels of the receiver antennas vary from 10.3 dBm to 9.3 dBm [19]. We focus on increasing the power of reciver antennas to 32 dBm.

Another experiment done by Meaney et al. represents a significant step toward clinical adoption of MWI by introducing a clinical prototype designed for breast cancer detection. The prototype combines advanced microwave hardware and signal processing algorithms to optimize imaging accuracy and reliability. The authors developed a clinically viable prototype that incorporates a conformal patient interface, facilitating accurate imaging of the breast in a comfortable and reproducible manner. The system uses microwave frequency bands to measure dielectric properties of the breast tissues. It provides quantitative maps of these properties, aiding in distinguishing malignant from benign tissues. An innovative algorithm based on iterative reconstruction was implemented, improving spatial resolution and contrast while compensating for complex scattering effects in heterogeneous tissues. The prototype was tested in a clinical environment to evaluate its performance. Initial results demonstrated the system's capability to identify regions of interest in the breast and its potential to complement existing diagnostic tools. His main challenge was the accurate reconstruction of dielectric profiles in the presence of noise and artifacts, the influence of breast shape and size on imaging performance, and the ability to differentiate between benign and malignant abnormalities[20].

2.3 Simulation Studies

Simulation studies play a crucial role in the development and evaluation of microwave breast cancer detection systems. One study utilized CST Microwave Studio to design a hemispherical breast model equipped with two micro-strip patch antennas. In this setup, the transmitter antenna remains stationary, while the receiver antenna is moved incrementally from the bottom to the top of the breast model to capture different data points [21].

Another study employed CST Microwave Studio to simulate a breast model using a monopole antenna. This antenna forms a synthetic circular array around the breast model and operates in a radar configuration, sending and receiving signals at each position [22]. A further study conducted in CST Microwave Studio involved simulating a breast detection setup using a hemispherical breast model and two horn antennas. The transmitter antenna emits a plane wave, while the receiver antenna captures the transmitted signal on the opposite side of the model. This study examined breast models of ten different sizes, with spherical tumors encased in limestone placed within the fibrous glandular layer of the model. [23].

Another innovative approach combined a wavelet transform reconstruction algorithm with a neural network, simulated using CST Microwave Studio. This simulation involved a three-dimensional heterogeneous breast model composed of fibrous glandular tissue, milk ducts, fat, and connective tissues. The dielectric properties of the breast model were calculated using a first-order Debye dispersion model. A plane wave was transmitted through the breast tissue, and probes were employed to receive the transmitted signal [24].

Similarly, Sultani et al. uses Microwave Thermoacoustic Imaging (MTAI)- a hybrid imaging modality that combines the strengths of microwave and ultrasound techniques. This technology leverages the distinct dielectric properties of malignant and healthy tissues and provides an opportunity to overcome the limitations of traditional imaging methods. They used COMSOL Multiphysics software for their simulation. MTAI is based on the conversion of electromagnetic energy (microwaves) into acoustic signals via thermoelastic expansion. Breast tissues are exposed to low-power microwave pulses. Malignant tissues, with higher dielectric properties, absorb more microwave energy than healthy tissues. The absorbed energy generates localized heating, causing thermoelastic expansion, which in turn produces acoustic waves. The acoustic waves are captured by ultrasound transducers and processed to reconstruct images that highlight the locations of abnormal tissues. The input source for this experiment was a port which produced microwave radiation. He provided 1000 W, 1 ms power pulse to the model which doesnot seem to be feasible in real life, as it would result in higher SAR and damaged skin tissues. Also, for this rated power, the rise in temperature is very low having temperature difference of only 0.005deg C. This led us to conclude that

temperature is not an important variable for microwave imaging[25].

2.4 Data Mining

In literature, many various studies about the data mining algorithms usage in cancer analysis have done until this time. Cancer analysis is one of the most important issues in the medical area. This problem also is one of the most examined problems. Some analysts have centered on achieving to obtain satisfactory results. To diagnose breast cancer, many studies including machine learning, artificial intelligence, data mining, etc., are used. The Random Forest(RF) algorithm can be used for classification in many areas including Health/Medical. The article of Ramon Diaz-Uriarte and Sara Alvarez de Andres [26] highlights that random forest is well-suited for micro array data due to its excellent performance even when most predictive variables are noise, its applicability to problems with more than two classes and its ability to return measures of variable importance. In the paper of Vibha et al. [27], a Decision Forest Classifier (DFC), which is based on the Random Forest classifier, was proposed for classifying mammograms. The data consisted of 200 instances were grouped into normal, benign and malign categories. The k-fold cross-validation method was used in this mentioned paper. According to the results of that paper, the proposed algorithm was performed with the accuracy of nearly 90.45

2.5 Microwave Imaging

In microwave breast cancer detection, Differential Calibration is a common technique that compares signals from a healthy breast to identify tumor responses. However, it is not useful when there is no prior data from a healthy breast for comparison (Porter et al., 2011) [28]. A one of the more efficient method is In-Place Calibration, where two receivers placed at the same distance from the transmitter capture signals simultaneously. This technique removes unwanted signals like skin reflection and antenna noise, allowing for more accurate detection of tumor responses, which have a slight delay (Kwon et al., 2016)[5]. Another approach, Array Rotation Calibration, involves rotating the antenna to capture two sets of signals and subtracting one from the other to remove noise (Klemm et al., 2009) [29]. After calibration, algorithms like Delay

and Sum (DAS) are used to reconstruct images. DAS works by combining signals from multiple receivers to create clearer, more detailed images of the tissue, helping in the detection of tumors (Shao et al., 2005) [30].The working of DAS algorithm can be summarized in the flowchart 2.1:

Additionally, the Merits open source algorithm has been utilized for more efficient

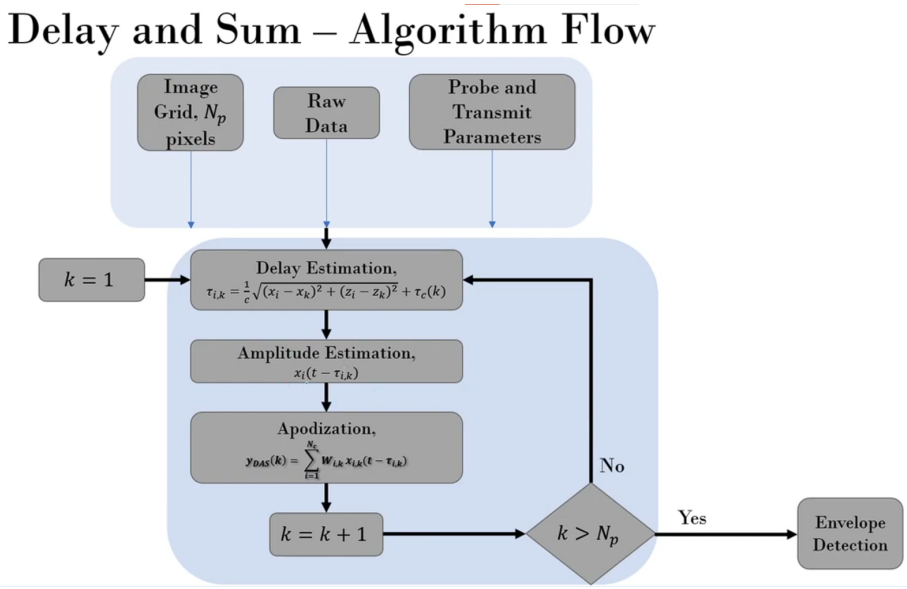

Figure 2.1: DAS Time Domain

image reconstruction, offering enhanced accuracy and speed in tumor detection with optimize signal processing techniques [31].

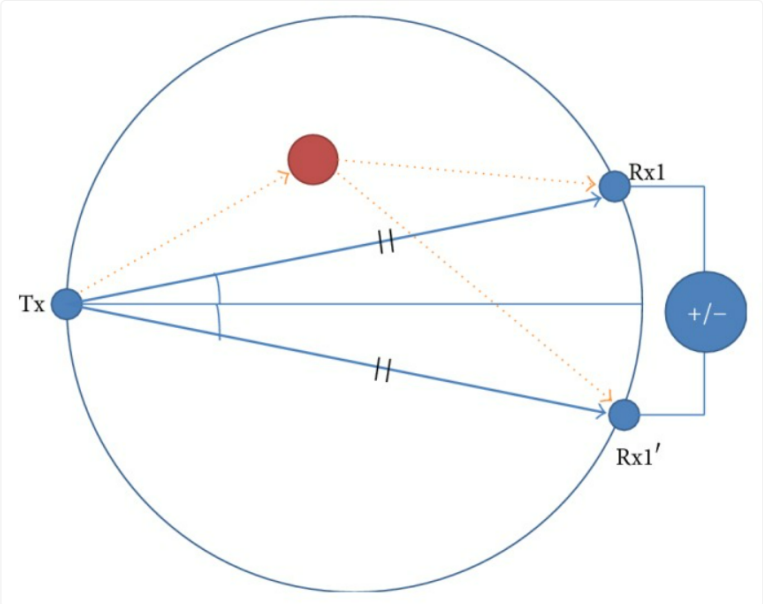

Figure 2.2: In-Place Calibration for Microwave Imaging, adapted from [5].

CHAPTER 3:
METHODOLOGY

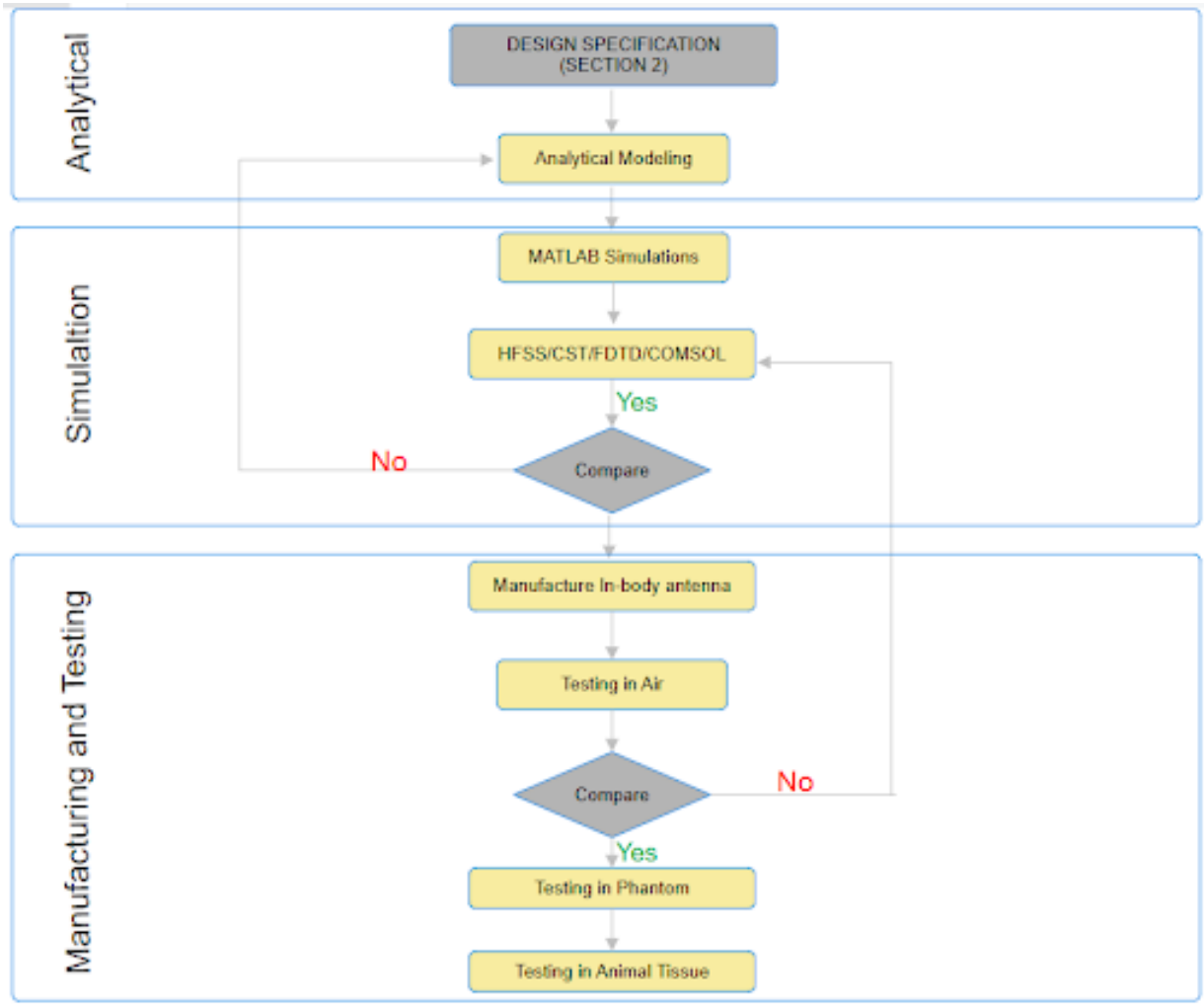

Figure 3.1: Design Flowchart

3.1 Phase I: Analytical Modeling of Patch Antenna

3.1.1 Introduction

A metallic strip or patch mounted on a dielectric layer(substrate) which is supported by ground plane is known as micro patch antenna. It has three parts respectively metallic patch with a very small thickness, the dielectric substrate and large metallic ground plane. Generally, the radiating patch is made of a dielectric substrate material. The dielectric substrate material consists of two sides: one side radiating patch and another side ground plane. Although high dielectric constant with thin substrate derogates unwanted radiation, it is not like better because of the greater loss of results in less efficiency and smaller bandwidth. The top layer (patch) is the conductive layer of the antenna, which can be generally made of gold, silver or copper. In this stage, the patch structure of the antenna is copper. The dielectric base is an optional insulating material with a wide range of fluctuating properties. The patch part and the ground part act as a transmission line and serve as a guide for the energy generated by the TEM waves. The thickness of the dielectric material generally ranges from 0.005 to 0.635 cm. Materials such as alumina, quartz, PTFE (polytetrafluoroethylene) are used for microwave circuits, but they are generally not preferred because they are expensive.

3.1.2 Parameters of Antenna

Analytical modeling focuses on predicting:

- Impedance: The approximate value of impedance of a transmitter, when equals the approximate value of the impedance of a receiver, or vice versa, it is termed as Impedance matching. Impedance matching is necessary between the antenna and the circuitry. The impedance of the antenna, the transmission line, and the circuitry should match so that maximum power transfer takes place between the antenna and the receiver or the transmitter. Its SI unit is ohm.

- Radiation Pattern: It is a graphical depiction of the relative field strength transmitted from or received by the antenna, and shows sidelobes and backlobes.

- Gain: It is a measure of the ability of the antenna to direct the input power into

radiation in a particular direction and is measured at peak radiation intensity.

$$Gain = \eta_e \times D$$

- Directivity: The ratio of maximum radiation intensity of the subject antenna to the radiation intensity of an isotropic or reference antenna, radiating the same total power is called the directivity. The directivity of a non-isotropic antenna is equal to the ratio of the radiation intensity in a given direction to the radiation intensity of the isotropic source.

$$Directivity = \frac{\text{Maximum radiation intensity of subject antenna}}{\text{Radiation intensity of an isotropic antenna}}$$

$$D = \frac{U_{max}}{U_o}$$

- Bandwidth: Range of frequencies over which the antenna operates effectively. The signal when transmitted or received, is done over a range of frequencies. This particular range of frequencies are allotted to a particular signal, so that other signals may not interfere in its transmission.

- Reflection Coefficient (S-parameters): The reflection coefficient is a measure of the ratio of the power of a forward signal that is reflected from a port compared to the total power of the signal minus what is lost as radiation. In terms of characteristic impedance to load impedance, the reflection coefficient is mathematically determined using the following equation:

$$\Gamma = \frac{Z_L - Z_o}{Z_L + Z_o}$$

  Where Γ is the reflection coefficient, Z_L is the load impedance, and Z_0 is the characteristic impedance of the transmission line or waveguide. For maximum energy transfer, it is desirable to have a reflection coefficient as close to zero as possible. The VSWR is mathematically derived from the reflection coefficient.

- Efficiency: Antenna Efficiency is the ratio of the radiated power of the antenna to

the input power accepted by the antenna. Simply, an Antenna is meant to radiate power given at its input, with minimum losses. The efficiency of an antenna explains how much an antenna is able to deliver its output effectively with minimum losses in the transmission line.

$$\eta_e = \frac{\text{Power radiated}}{\text{Power Input}}$$

The conductive layers of the micro strip antennas greatly affect antenna parameters and antenna performance such as bandwidth, antenna gain, loss of return, directivity, etc.

3.1.3 Working of Patch Antenna

A micro strip patch antenna radiates from fringing fields around its peripheral surfaces as shown in 3.2. When the metallic patch is excited by feed, a charge distribution is being established between the ground plane an underneath of the patch. There is a positive charge below the patch and the ground plane is discharged to negative. Because of that, attractive forces are being set up between the patch and ground plane. We assume the four side walls of the substrate as the magnetic walls through which radiation takes place.The inside area of the dielectric substrate is presented as a cavity limited by the electric walls(copper plate on the top and bottom of the substrate). The field inside the cavity is assumed equal to zero, and its influence in the infinite region outside is represented by the equivalent surface current on the surface of the cavity. Impedance matching occurs when a patch resonates as a resonant cavity. The antenna can achieve peak efficiency with perfect impedance matching.

The current is maximum at the center of the patch, while the electric field is maximum

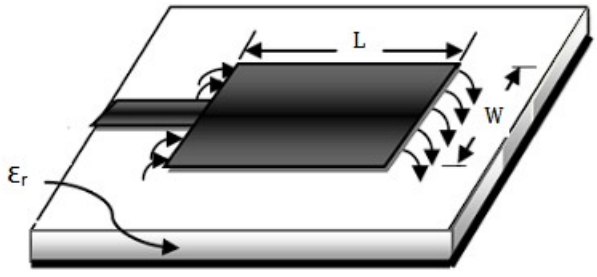

Figure 3.2: Rectangular Patch Antenna

at the radiating edges. The tangential magnetic field components at the slots is zero. A thick dielectric substrate having a low dielectric constant i desirable for antenna design because this provides better efficiency, larger bandwidth and better radiation. Although such configuration leads to larger antenna size. To design a compact patch antenna, higher dielectric constants must be used, which are less efficient and result in narrower bandwidth. Therefore, a compromise must be reached between antenna dimensions and antenna performance.

Fringing effect in Micro Patch Antenna

When we feed antenna with respect to ground, electromagnetic waves gets coupled from patch antenna to ground. At, the edges EM waves goes to space before going to the ground. This is known as fringing effect. Because of fringing, antenna radiates in space. To increase fringing, there are three ways:

- Low dielectric constant substrate
- Increase height of subtrate
- Increase width of substrate.

Fringing increases the effective electrical length of the patch, which reduces the resonant frequency compared to what the physical length suggests. This allows designers to calculate the resonant frequency more accurately by considering the extension caused by fringing. Considering 3.4, because of fringing there is increase in effective length

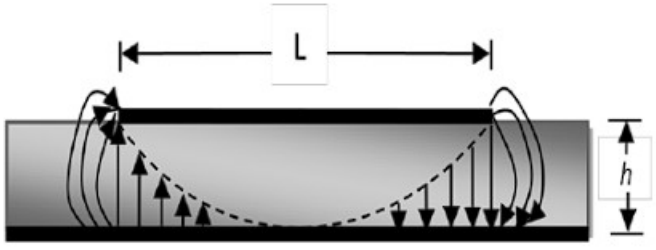

Figure 3.3: Fringing effect on antenna

of the patch on both sides. Thus, the effective length becomes:

$$L_{eff} = L + 2\Delta L$$

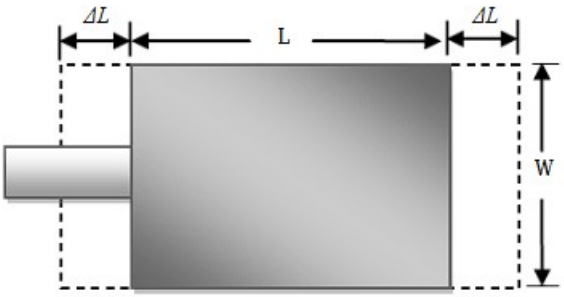

Figure 3.4: Change in effective length due to fringing

And the resonating frequency becomes:

$$f_r = \frac{c}{2L_{eff}\sqrt{\varepsilon_{eff}}}$$

$$f_r = \frac{c}{2(L+2\Delta L)\sqrt{\varepsilon_{eff}}}$$

The following formulas have been used to construct a mathematical model, which forms the fundamental design. This is the initial step in achieving the final design and then adjusting it to meet the required results.

Determining the Width(W) of antenna:

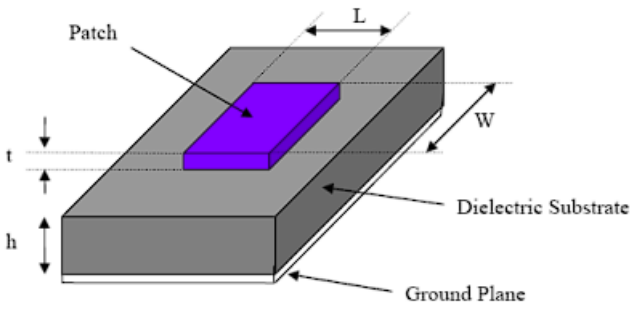

Figure 3.5: Basic Structure of Micropatch Antenna

$$W = \frac{c}{2f_o\sqrt{\frac{\varepsilon_r+1}{2}}} \tag{3.1}$$

Once the width is known; length of the antenna can be determined as:

$$L = \frac{c}{2f_r\sqrt{\varepsilon_e ff}} - 2\Delta L \tag{3.2}$$

Now, To find the height of substrate:

$$\frac{\Delta L}{h} = 0.412\frac{(\varepsilon_e ff + 0.3)(\frac{W}{h} + 0.264)}{(\varepsilon_e ff - 0.258)(\frac{W}{h} + 0.8)} \tag{3.3}$$

where,

the effective dielectric constant is:

$$\varepsilon_e ff = \frac{\varepsilon_r + 1}{2} + \frac{\varepsilon_r - 1}{2}[1 + 12\frac{h}{W}]^{-\frac{1}{2}}, \tag{3.4}$$

c is the speed of light,

f_r is the resonant frequency

$L_e ff$ is the resonating length

$\varepsilon_e ff$ is the effective dielectric constant

The feed line and feed width are another important parameter in designing the antenna. As proper tuning of feed length and its width gives better impedence matching of the antenna, as a result less VSWR and better power transfer. Thus, better approximation of characteristic impedence can be used to determine the feed width of the transmission line:

$$Z_c = \frac{60}{\sqrt{\varepsilon_{eff}}}\ln(\frac{8h}{W_o} + \frac{W_o}{8h}); for \frac{W_o}{h} <= 1 \tag{3.5}$$

$$Z_c = \frac{(120\pi/\sqrt{\varepsilon_{eff}})}{\frac{W_o}{h} + 1.393 + 0.667\ln(\frac{W_o}{h} + 1.444)}; for \frac{W_o}{h} > 1 \tag{3.6}$$

Similarly, the feed line length can be calculated using formula:

$$l = \frac{\lambda}{4\sqrt{\varepsilon_{eff}}} \tag{3.7}$$

3.2 Phase II: Simulation

3.2.1 Designing of Antenna

Before actual fabrication of the antenna, simulation is required to know if the antenna's dimensional parameters obtained from the formula is correct and the antenna resonates within the required frequency. The simulation model was prepared in CST software. The dimension of the proposed antenna was measured to be $58 \times 76 \times 1.6mm^3$. The remaining parameters are shown in table 3.1:

Parameters	**Value (mm)**
substrate thickness	1.6
patch length	29
patch width	38
substrate length	58
substrate width	76
ground thickness	0.035
inset length	8.85
inset width	5.137
feedline length	23.35
feedline width	3.137

Table 3.1: Dimensions of Antenna

The simulated antenna is shown in figure 3.6.

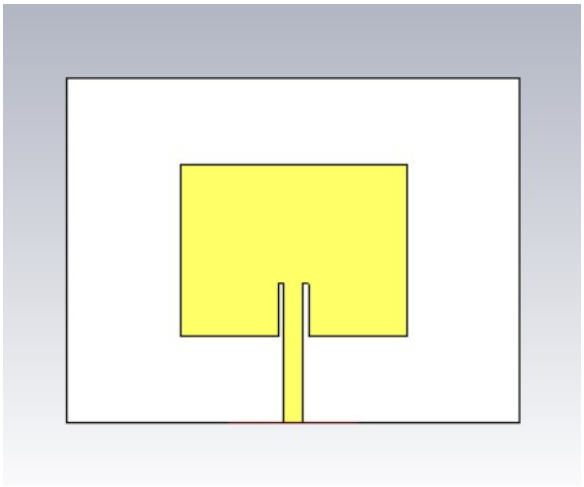

Figure 3.6: Front view of antenna

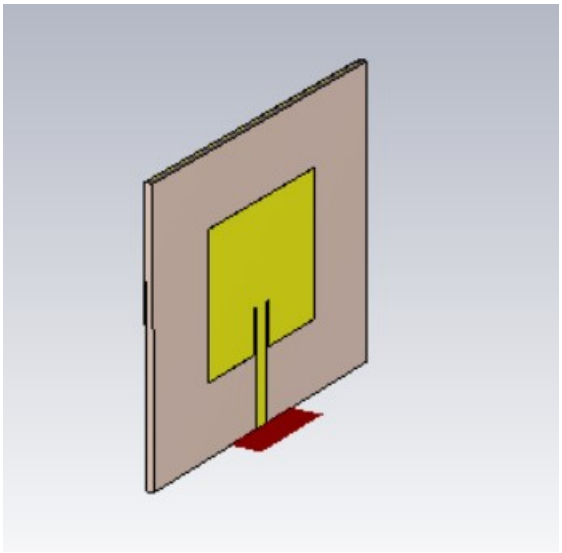

Figure 3.7: Isometric view of antenna

3.2.2 Designing the phantom

The breast phantom as shown in Figure3.8 is created in CST software. The phantom is designed to be as close as real breast. Different layers of breast included in the design is explained briefly:

- Skin: It is the outermost layer, providing a protective covering for the breast tissue. It contains sweat glands, sebaceous (oil) glands, and hair follicles. It is shown by brown color in the model.

- Nipple: The nipple is in the center of the breast, and it's surrounded by the areola. Each nipple contains milk duct openings through which breast milk flows. Nipples are held erect by small, smooth muscles that respond to signals from your autonomic nervous system[32]. They are dense as it contains lots of duct and lymps openings that connects to the mammary glands. For simulation, its electrical properties are kept similar to that of skin except the density is differed.

- Adipose Tissue (Fat Layer): This layer provides cushioning and shape to the breast. Its thickness varies depending on age, hormonal status, and body composition. It is shown by yellow color in the phantom.

- Fibro Glandular Layer: Also known as Mammary layer, this is the functional part of the breast. Each breast has 15–20 lobes, divided into smaller lobules that produce milk. Milk Ducts carry milk from the lobules to the nipple during

breastfeeding. All the connective tissues, ducts, lymph nodes, nerves, muscles, glands and blood vessels are shown by a compact layer which is shown by pink colour in the phantom.

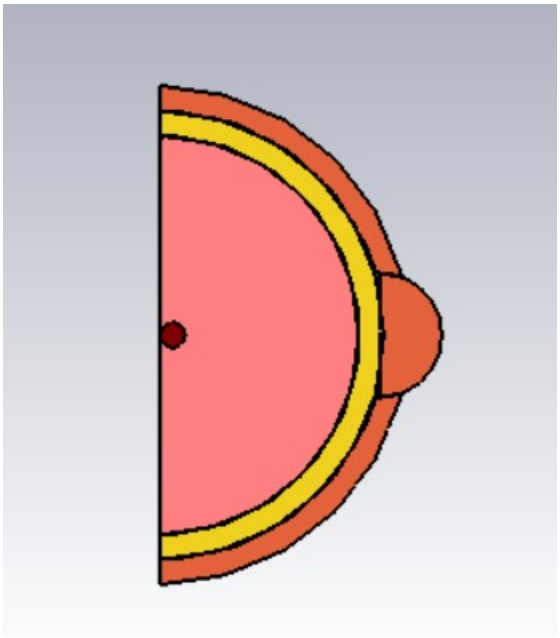

Figure 3.8: Designed Breast Phantom

Tissues	Electrical properties					
	Dielectric (ε_r)	***Conductivity*** σ (s/m)	***Mass density*** (Kg/m3)	***Thermal Conductivity [W/K/m]***	***Heat Capacity [KJ/K/Kg]***	***Mue***
Skin	36.7	2.34	1109	0.37	3.391	1
Adipose	4.84	0.262	911	0.21	2.348	1
Glandular	50	3.46	1041	0.33	2.960	1
Tumor	50.9	4	1058	_	_	1

Figure 3.9: Electrical Properties for different layers of Breast

3.3 Phase III: Fabrication and Testing

After the simulation process, fabrication is done. The fabrication of antenna was done through etching process. The feed line of antenna was connected to the SMA(Sub Miniature Version A) connector which is further connected to the VNA(Vector Network Analyzer) through RF coaxial cable. The testing of antenna is done using NanoVNA. The fabricated antenna is shown in 3.10

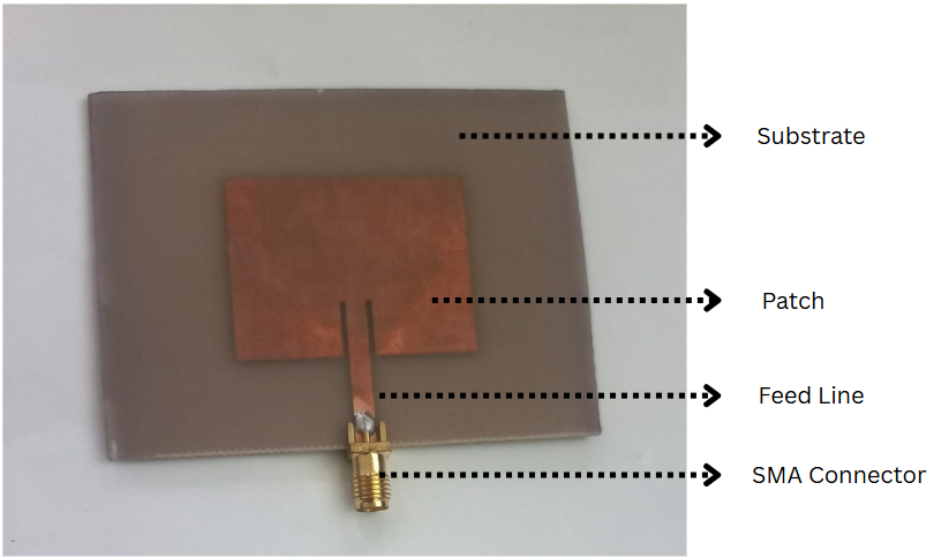

Figure 3.10: Fabricated Antenna

3.3.1 VNA (Vector Network Analyzer)

A vector network analyzer, is a type of network analyzer that measures the magnitude and phase of multiple frequencies at the same time. This makes vector network analyzers more accurate than scalar network analyzers. This information can be used to calculate the impedance of the network, as well as the isolation and coupling between ports. Vector network analyzers typically use a technique called vector analysis to measure the impedance of a network. In vector analysis, the magnitude and phase of each impedance are measured independently, and the results are combined to calculate the impedance of the network. Vector network analyzers are used in a variety of applications, including antenna testing, filter design, and microwave circuit design. They are used to characterize the performance of RF and microwave components and systems

and can measure insertion loss, return loss, and S-parameters of RF and microwave devices and systems. A VNA consists of a signal generator, a mixer, a detector, and a display. The signal generator produces a signal of known frequency and amplitude, which is applied to the input of the network under test. The mixer mixes the signal from the generator with a reference signal, and the detector measures the signal that is output from the mixer.

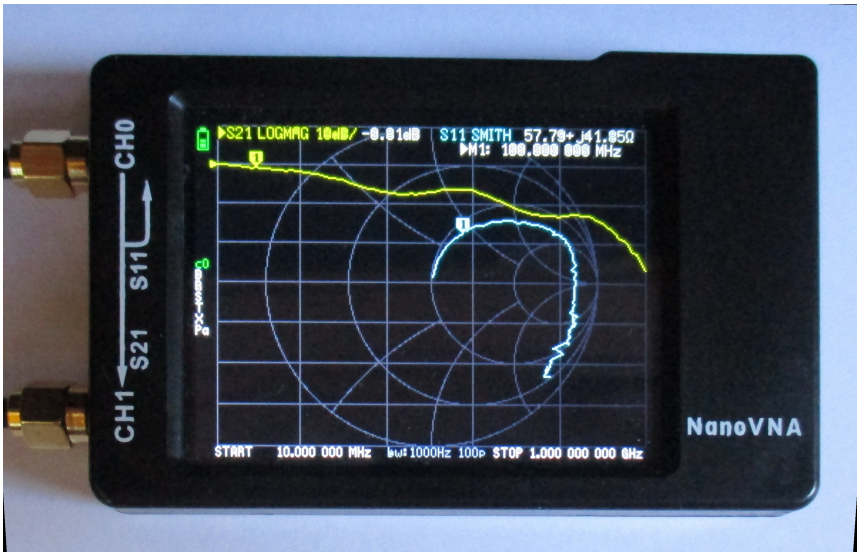

Figure 3.11: NanoVNA

3.3.2 Parameters measured using VNA

i. **S parameters**

S-parameters also known as Scattering Parameters is used for analysis of microwave components, RF circuits and Antennas.S-parameters are a type of mathematical function that describes the behavior of a two-port network. They are derived from the network's scattering matrix, which is a mathematical representation of the network's response to an arbitrary input. The scattering matrix is a square matrix, and the S-parameters are the column vectors of its eigenvalues[33].

It is used for such purposes because at microwave frequency, it is not possible to have open circuit and short circuit. Equipments are not available to measure voltage and current. Active devices like microwave transistor, tunnel diode, TRAPIT diode,etc have issues of stability. Because of these reasons, we don't do analysis of microwave components using Y, Z, A, B, C and H-parameters. S-parameters is

measured using formula:

$$S_{ij} = \frac{\text{Normalized Reflected wave at i Port}}{\text{Normalized Incident wave at j port}}$$

$$S_{ij} = \frac{b_i}{a_j}$$

where,

$$b_i = \frac{\text{Reflected Voltage at i port}}{\sqrt{Z_{oi}}}$$

$$a_j = \frac{\text{Reflected Voltage at j port}}{\sqrt{Z_{oj}}}$$

Z_{oi}: Characteristics Impedance of i port

Z_{oj}: Characteristics Impedance of j port

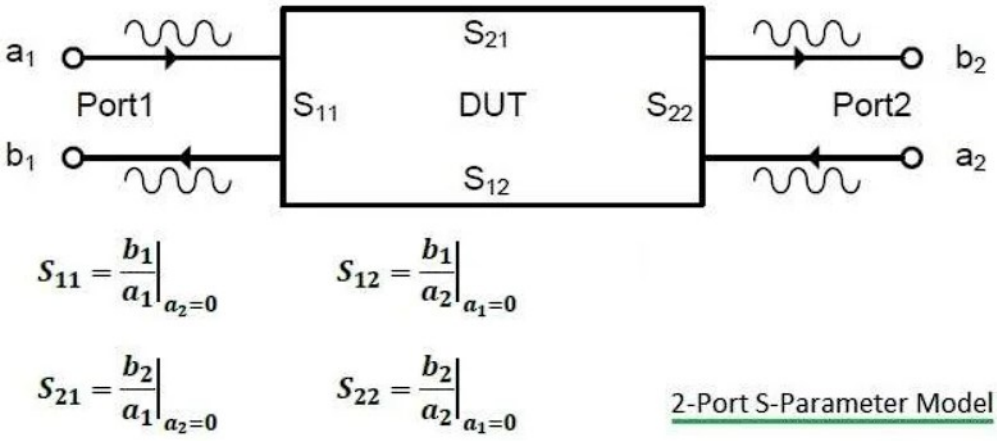

Figure 3.12: S Parameter of Two Port Network

Thus, S matrix for 2 port networks becomes: [S]= $\begin{bmatrix} S_{11} & S12 \\ S_{21} & S_{22} \end{bmatrix}$

S parameters measures the return loss and transmission loss of the DUT. Return loss (RL) is a measure of how much energy is reflected back from a discontinuity in a transmission line, expressed in decibels. It is one of the important parameters that is used to characterize the performance of a transmission line. The higher the return loss, the better the line performance. A transmission line can be discontinuous in many ways: at a connector, at a load, or at a junction. In each case, energy is reflected back from the discontinuity[34]. The return loss is the ratio of the power that is reflected back to the power that is transmitted. S11 measures the return loss at port 1.

Networks analyzers measures the performance of a communication network by injecting a signal into one end of the network and measuring the signal at the other end. Insertion loss is the loss of signal power that occurs as the signal travels through the network. This loss is caused by the resistance of the wires in the network, the mismatch of the impedance of the wires, and the loss of power in the signal due to radiation and absorption. The insertion loss can be measured in decibels (dB). S21 measures the transmission loss at port 2.

If S_{11} = 0dB, then all the power is reflected from the antenna and nothing is radiated. If S_{11} = -10dB, this implies that if 3dB of power is delivered to the antenna, 7dB is the reflected back.

ii. **VSWR**

The voltage standing wave ratio (VSWR) is a measure of the impedance matching of a load to a source. It is the ratio of the maximum voltage amplitude to the minimum voltage amplitude at any point along the line. The higher the VSWR, the worse the match. Impedance mismatch can cause reflections, which can lead to signal distortion and loss. If we suppose, port 1 to be input and port 2 to be output with their corresponding impedances of Z_{in} and Z_{out}, then reflection coefficients at their corresponding port becomes:

$$\Gamma_1 = \frac{Z_{in} - Z_{01}}{Z_{in} + Z_{01}} \tag{3.8}$$

$$\Gamma_2 = \frac{Z_{out} - Z_{02}}{Z_{out} + Z_{02}} \tag{3.9}$$

$$\text{Return loss} = -20\log|\Gamma| \tag{3.10}$$

Thus, VSWR can de determined using 3.10 as:

$$VSWR = \frac{1+|\Gamma|}{1-|\Gamma|} \tag{3.11}$$

iii. **Smith Chart**

Smith Chart is simply a graphical calculator for computing impedance as a function of reflection coefficient. The diagram consists of constant resistance circle, constant reactance circle, wavelength towards generator and wavelength towards load. This diagram also helps to determine the angle of reflection coefficient.

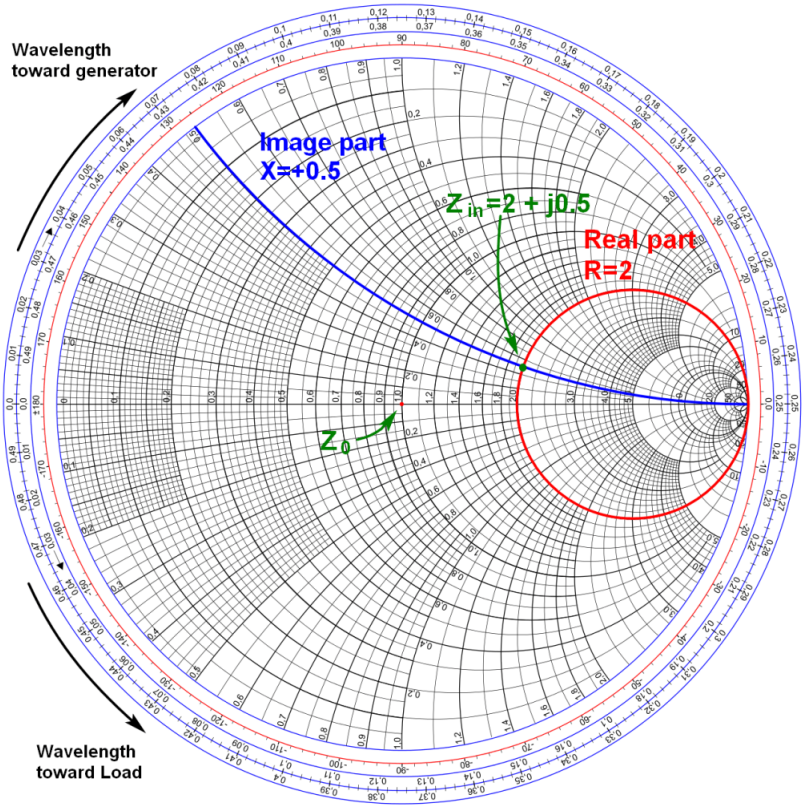

Figure 3.13: Smith Chart

3.3.3 Calibration of VNA

Calibration of a vector network analyzer (VNA) is the process of adjusting the VNA's measurements to correspond to a specific known impedance. The calibration procedure ensures that the VNA's measurements are accurate and repeatable. The calibration of VNA is done by connecting the testing port to open pin, short pin, load pin and thru pin consecutively.

3.4 Flowchart showing Data transfer in Antenna

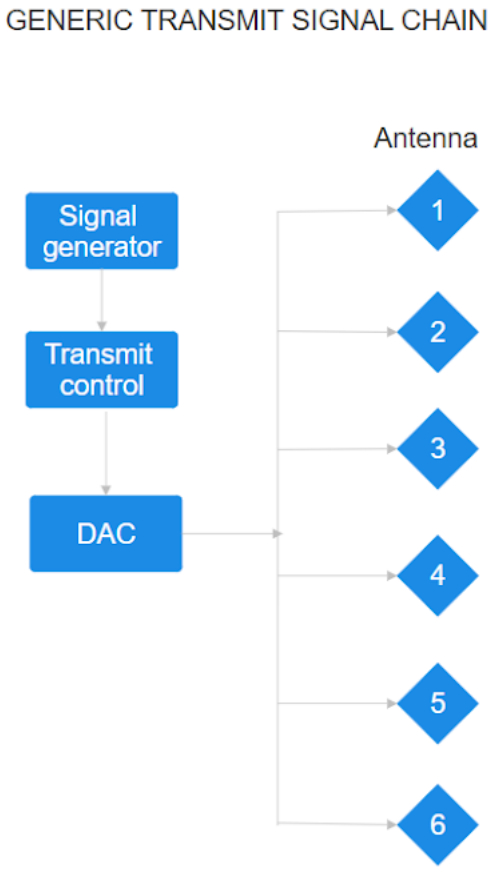

Figure 3.14: Transmit Chain

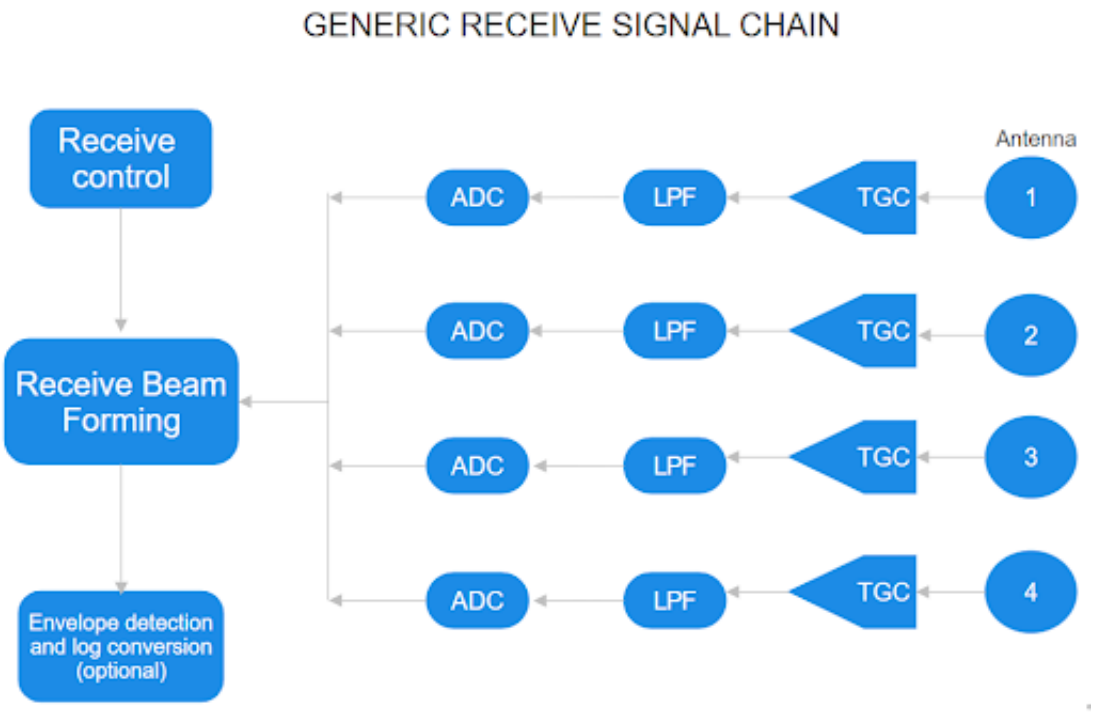

Figure 3.15: Receive Chain

CHAPTER 4:
RESULTS AND DISCUSSION

This chapter focuses on the output and results obtained from the antenna in simulation and real time environment.

4.1 Comparison of S parameters

The S parameters of a single antenna obtained from the simulation and VNA in real environment is shown in 4.1a and in 4.1b From figure 4.1a, we can see that the antenna

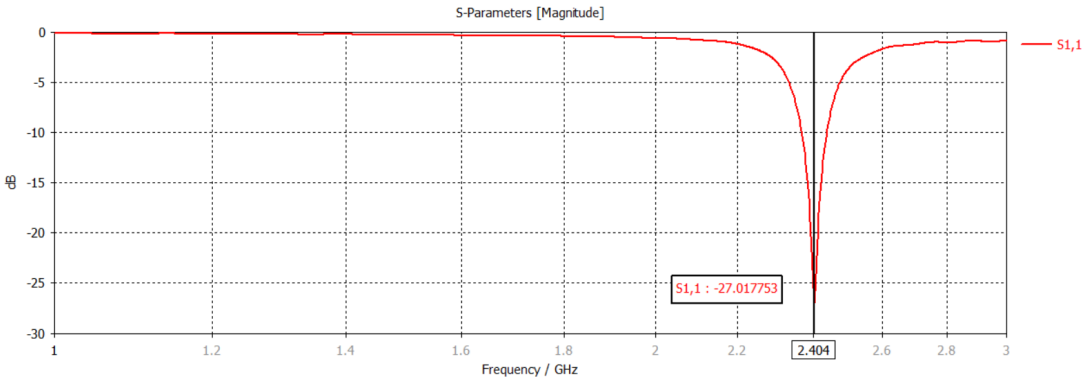

(a) S11 of antenna from CST simulation

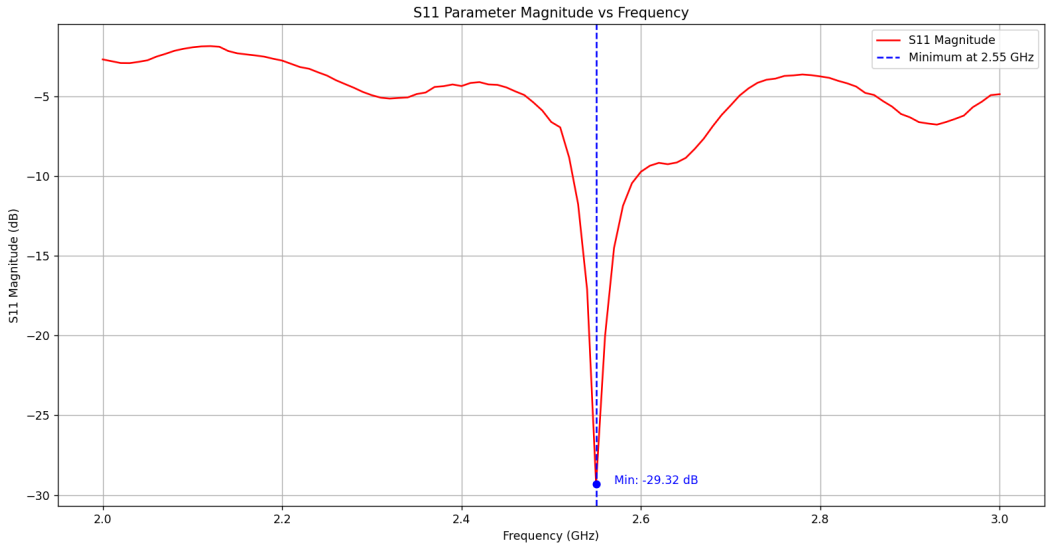

(b) S11 of antenna from VNA

resonates at 2.404 GHz which is the desired resonating frequency. The return loss is -27.015 dB. Antenna is said to good if the S11 parameter is less than -15 dB.

The figure 4.1b, shows that the fabricated antenna resonates at 2.55 GHz. However, the

return loss is less compared to the simulation antenna. The shift in resonating frequency may be because of following reasons:

- The roughness of the conductive material on the antenna (e.g., copper) can introduce slight changes in the antenna's impedance and resonating frequency
- Variations in dimensions during the etching process can lead to changes in the resonating frequency. For instance, slight deviations in the length, width, or thickness of the antenna or its substrate can shift the frequency.
- The substrate we chose may not be purely FR4. Hence, difference in the dielectric constant may result in change in resonating frequency.
- The method of connecting the antenna to the feed line introduces parasitic inductance or capacitance, which can detune the antenna slightly.
  The simulated antenna had impedance of 50Ω, while the fabricated antenna showed impedance of 43Ω-4.57j. There seems to be little loss in the form of reactive impedance. From these parameters we conclude that this antenna is perfect for output setup. Two antennas were fabricated to make one transmitting and another receiving antenna. The parameters of second antenna was similar to that of the first.

4.2 Arrangement of two antennas

It is required for the transmitting and receiving antenna to have maximum power transfer. This is possible when there is impedance matching between them. For this, we kept antennas 20 cm apart for initial experimental setup and later kept at 10cm apart. The VNA was calibrated for port 0 and port 1. The antenna was then connected and kept still for a minute and result was taken. The result is shown in figure 4.2. The figure shows that the return loss at port 0 is -21.64dB This means 7.9% of the input power is reflected, and the remaining 92.1% of the input power is transmitted into the device.
and later in the glass enclosed environment return loss drop to -25.28dB as shown in figure 4.3 S21 is often used to analyze how well an antenna couples with another antenna. S21 = -20dB suggests weak coupling or poor signal transmission. This may be because the setup was not properly isolated. The impedance is 43.3Ω, which is satisfactory.

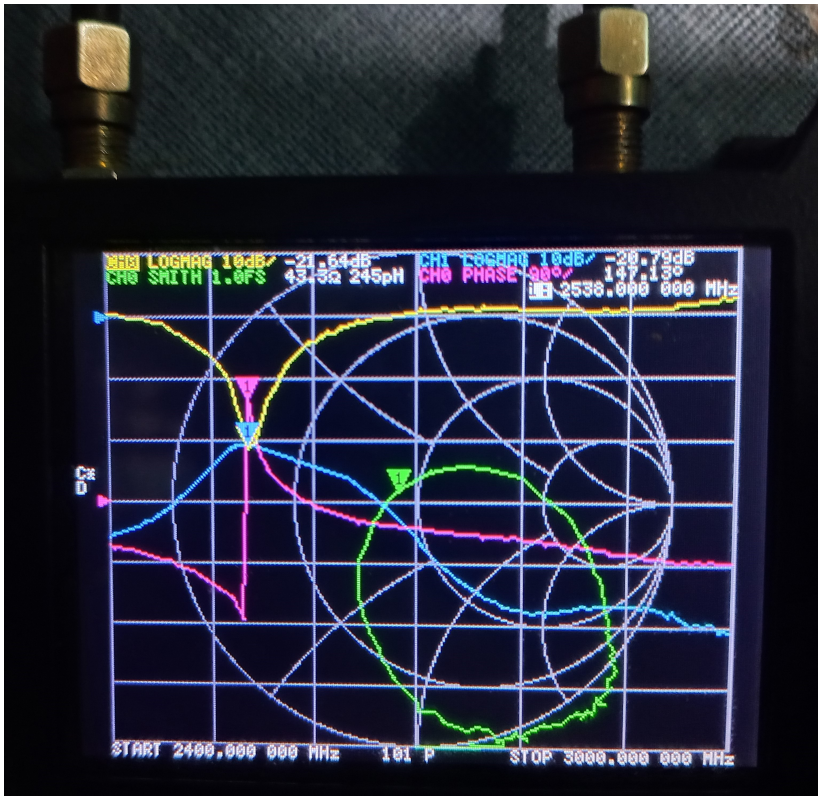

Figure 4.2: Parameters of two antennas in VNA

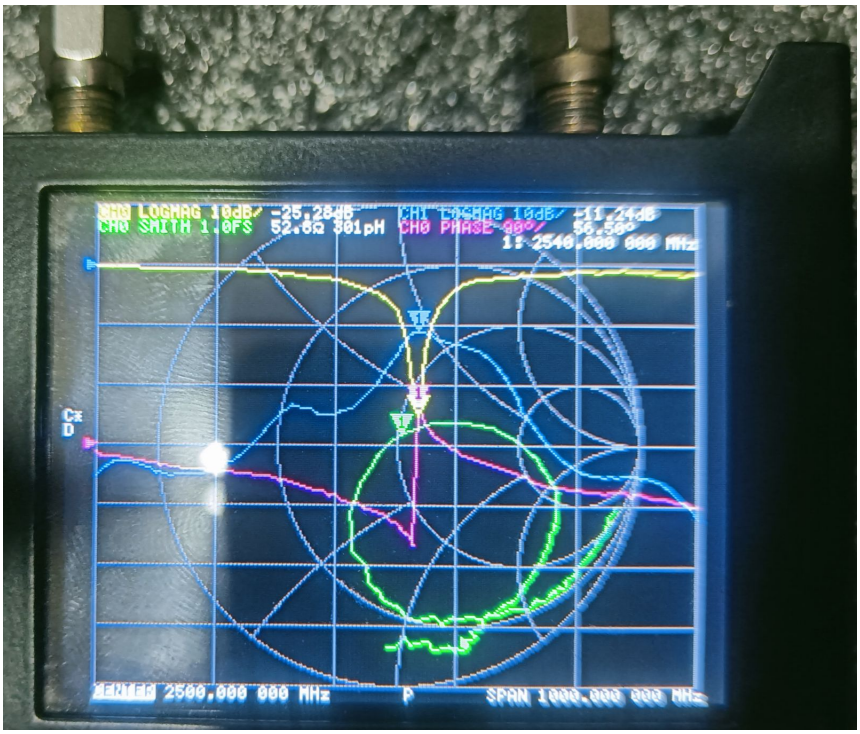

Figure 4.3: Parameters of two antennas at glass enclosed setup in VNA

4.3 Microwave Imaging from Scattering Parameters

4.3.1 Introduction

The detection of breast cancer using microwave signals is based on the differences in the scattering properties of malignant and normal breast tissues. These differences arise primarily due to the varying water content in the tissues. Malignant tumors generally have a higher water content, which results in a larger scattering cross-section compared to normal fatty tissues. This property allows microwave-based imaging techniques to detect tumors by analyzing the microwave signal interactions with breast tissues.

4.3.2 Microwave Scattering Properties of Malignant and Normal Breast Tissues

Hagness et al. [16] demonstrated that malignant tumors, which possess higher water content, exhibit significantly larger microwave scattering cross-sections than normal breast tissues, which are mainly composed of fat and have a lower water content. This difference in microwave scattering behavior is critical for non-invasive breast cancer detection methods. The dielectric properties of tissues, including the relative permittivity (ε_r) and electrical conductivity (σ), differ considerably between normal and malignant breast tissues. Gabriel et al. [17] reported that normal breast tissues have a relative permittivity of around $\varepsilon_r = 9$ and a conductivity $\sigma = 0.4$ S/m. In contrast, malignant tumors exhibit much higher values, with $\varepsilon_r = 50$ and $\sigma = 4$ S/m. This increase in permittivity and conductivity is attributed to the tumor's higher water content, which significantly influences the propagation of microwave signals in the tissues.

4.4 System Setup in CST Microwave Studio

To simulate the interaction of microwave signals with breast tissues, a simple breast model was created using CST Microwave Studio. This model represents a hemisphere with a radius of 60 mm, simulating the general structure of the breast tissue.

The transmission and reception of microwave signals was carried out using a four-microstrip patch antenna system. The antennas are positioned at the following coordinates in the simulation space:

- **Antenna 1**: Located at (-105, 19, 45.25) mm

- **Antenna 2**: Located at (19, 105, 45.25) mm
- **Antenna 3**: Located at (105, -19, 45.25) mm
- **Antenna 4**: Located at (-19, -105, 45.25) mm

4.5 Microwave Signal Transmission and Reception

- The four microstrip patch antennas transmit and receive microwave signals.
- Scattering parameters such as **reflection coefficient** (S_{11}) and **transmission coefficient** (S_{21}) are measured.
- These parameters evaluate microwave signal interaction with the **breast phantom**, especially around potential tumor regions.

4.6 Breast Phantom Design based on the property 3.9

- **Structure**: Multi-layered phantom mimicking human breast tissue properties.
- **Layers**: Includes skin, adipose (fat), glandular tissue, and a tumor inclusion.
- **Operating Frequency**: 2-3 GHz for optimal penetration and resolution.

4.6.1 Skin Layer

- Dielectric constant (ε_r): 36.7
- Conductivity (σ): 2.34 S/m
- Mass density: 1109 Kg/m^3
- Thermal conductivity: 0.37 W/K·m
- Heat capacity: 3.391 KJ/K·Kg

4.6.2 Adipose (Fat) Tissue (Represented by Blue)

- Dielectric constant (ε_r): 4.84
- Conductivity (σ): 0.262 S/m

- Mass density: 911 Kg/m^3
- Thermal conductivity: 0.21 W/K·m
- Heat capacity: 2.348 KJ/K·Kg

4.6.3 Glandular Tissue (Represented by Yellow)

- Dielectric constant (ε_r): 50
- Conductivity (σ): 3.46 S/m
- Mass density: 1041 Kg/m^3
- Thermal conductivity: 0.33 W/K·m
- Heat capacity: 2.960 KJ/K·Kg

4.6.4 Tumor Inclusion (represented by Red)

- Dielectric constant (ε_r): 50.9
- Conductivity (σ): 4 S/m
- Mass density: 1058 Kg/m^3

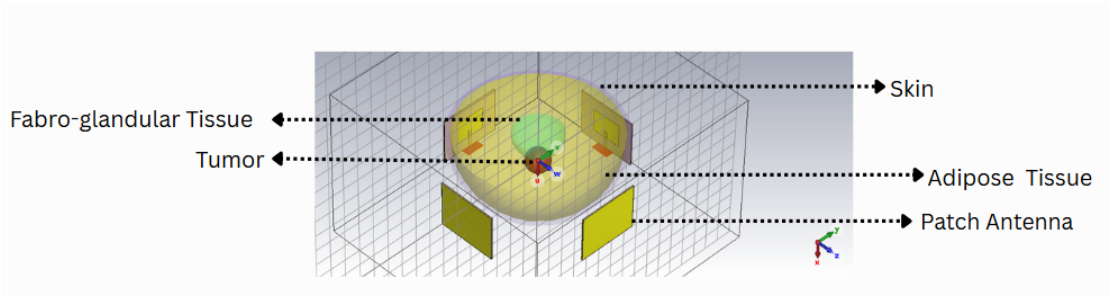

Figure 4.4: CST Microwave Studio Setup of Breast phantom Design for Simulation

4.6.5 SAR calculation

In our study, the maximum Specific Absorption Rate (SAR) value obtained was **0.683 W/kg** averaged over 10 grams of tissue, which is significantly below the safety guidelines set by global organizations:

- **ICNIRP (2020)[2]:** 2 W/kg averaged over 10 grams for the general public.
- **IEEE C95.1-2019:[3]** 2 W/kg averaged over 10 grams for uncontrolled environments.
- **FCC (USA):[4]** 1.6 W/kg averaged over 1 gram (stricter 1g averaging).

The measured SAR (0.683 W/kg over 10 g) is 65% lower than the ICNIRP/IEEE limit of 2 W/kg. Even under the FCC's stricter 1 g benchmark (1.6 W/kg), the system remains compliant. Moreover, since SAR values typically decrease when averaged over larger tissue volumes, the 10 g-averaged SAR inherently ensures safety for smaller averaging masses (e.g., 1 g).

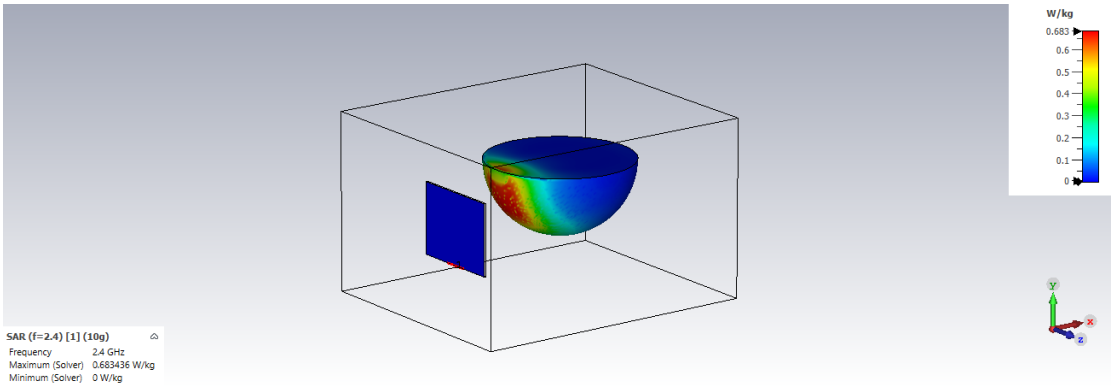

Figure 4.5: SAR Calculation in CST Microwave Studio Setup of Breast phantom

4.7 Microwave Imaging Flowchart

Below is a flowchart representing the workflow of the Microwave Imaging, starting from the development of the setup in CST Microwave Studio, through the simulation, signal processing, artifact removal, and image construction.

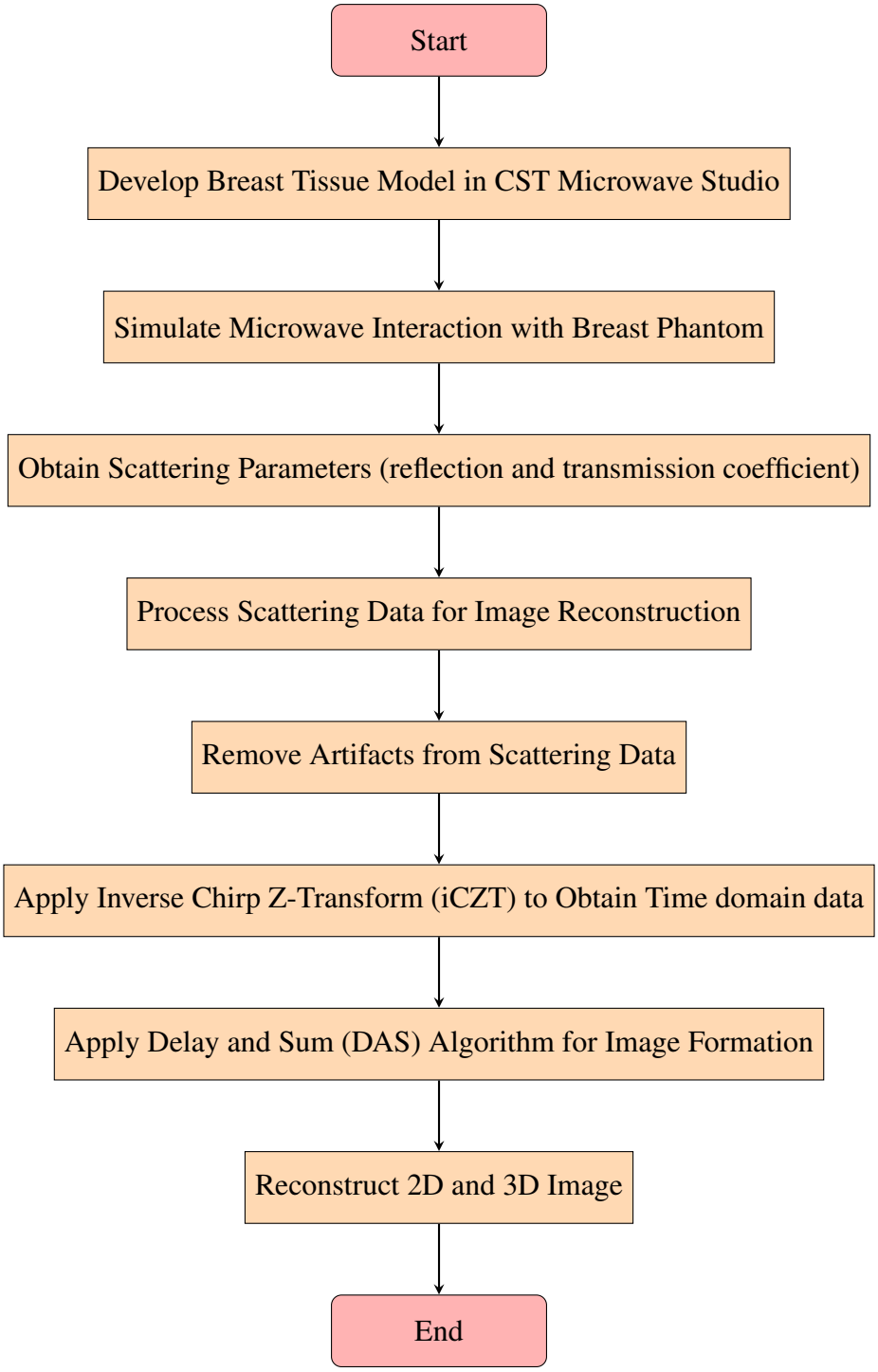

4.7.1 Signal Processing and Scattering Parameter Analysis

The scattering parameters are crucial for analyzing the interactions between microwave signals and breast tissues. These parameters help to evaluate the amount of signal that is reflected and transmitted at different points in the breast phantom, which is key to detecting potential tumor regions. The scattering data is then processed to help reconstruct an image of the internal tissue structure, which can reveal the presence of tumors. Once the scattering parameters are obtained, the next step is signal processing. Signal processing techniques are used to enhance the quality of the measured data and improve the accuracy of tumor detection.

The important aspect of signal processing is **artifact removal**, which is critical for ensuring the reliability of the reconstructed images. Artifacts in microwave imaging can occur due to factors like skin reflections or electromagnetic interference. These artifacts can obscure the real signal from the tumor or other tissues of interest.

We used a technique known as **Average Subtraction** to remove artifacts. This method works by subtracting the mean response across all channels from each individual channel. The assumption behind this technique is that the artifacts (such as skin reflections or incident pulses) are common across all channels, while the tumor signal varies from one channel to another. By removing the mean artifact response, the tumor signals are enhanced, leading to a clearer reconstruction [35].

One key technique used in this study is the **Inverse Chirp Z-transform (iCZT)**, which helps improve the spatial resolution of microwave signals, making it easier to distinguish between tumor and non-tumor tissues. The iCZT was preferred over the Inverse Fourier Transform (IFT) because the IFT assumes periodicity in the signal, which doesn't hold for the microwave signals interacting with breast tissue. Since the microwave scattering data is non-periodic, the IFT struggles to resolve fine spatial details. In contrast, the iCZT does not rely on periodicity and provides better resolution of the frequency spectrum, making it more suitable for accurately distinguishing tumors from surrounding tissue and enhancing the overall quality of the imaging.

Mathematically, the iCZT is an inverse operation that converts frequency-domain data into the time domain.

$$S(z) = \sum_{k=0}^{N-1} s(f_k) \cdot e^{j2\pi \cdot k \cdot \frac{\Delta f}{\Delta t} \cdot f_k}$$

where:

- $S(z)$: The transformed signal in the time domain.
- $s(f_k)$: Frequency-domain samples.
- Δf: Frequency increment.
- Δt: Time increment.
- f_k: Frequency samples.

This operation allows for high-resolution time-domain signals, which are crucial for distinguishing fine spatial details in breast tissue and enhancing the image reconstruction quality. The iCZT's ability to handle non-periodic data makes it especially effective for processing microwave scattering data in breast cancer detection.

4.7.2 Image construction with Delay-and-Sum (DAS)

After signal processing and artifact removal, the **Delay-and-Sum (DAS)** algorithm is applied to reconstruct the image of the breast tissue. This algorithm synthesizes the microwave signals from different antenna channels to produce an image that can indicate the presence of a tumor. The image reconstruction process plays a crucial role in visualizing the internal structure of the breast and identifying regions with abnormal scattering, which may be indicative of tumors.

The DAS algorithm relies on calculating the delays for signals from multiple antenna channels, aligning these signals, and summing them to enhance the image. For this study, the breast phantom has been discretized into **140,274 coordinate points**, each representing a location in the imaging domain. The mathematical steps involved in the DAS algorithm are as follows:

Delay Computation

The delays are calculated based on the distance between antennas and the point in the imaging domain. Let the speed of light in the medium be defined as:

$$v = \frac{c_0}{\sqrt{\varepsilon_r}}$$

where:

- c_0 is the speed of light in a vacuum ($299,792,458$ m/s),
- ε_r is the relative permittivity of the medium.

The time delay for a signal to travel from transmitting antenna t to a point P and then to the receiving antenna r is given by:

$$\tau(t,r,P) = \frac{\|P - A_t\| + \|P - A_r\|}{v}$$

where:

- P is the point in the imaging domain,
- A_t and A_r are the coordinates of the transmitting and receiving antennas, respectively,
- $\|\cdot\|$ represents the Euclidean distance.

Signal Alignment

Using the calculated delays, the received signals are adjusted (delayed or advanced) to align with a reference time. For a signal in the time domain $s(t)$, the delay operation is:

$$s'(t) = s(t - \tau)$$

where:

- τ is the calculated delay.

2D Image Formation

Once the signals are aligned, they are summed to produce an intensity value for each point in the imaging domain:

$$I(P) = \sum_{t,r} \left| s'_{t,r}(t) \right|$$

where $I(P)$ is the intensity at point P.

This process highlights areas with abnormal scattering, which may indicate the presence of tumors. The DAS algorithm is computationally efficient and widely used in microwave imaging applications for its simplicity and effectiveness.

4.7.3 Simulation Setup and 2D and 3D Image construction

To Reconstruct the image using the S-parameter,The simulation setups were created with the transmitting and receiving antennas positioned at two different locations mentioned above. The imaging domain was divided into **140,274 coordinate points**, and the DAS algorithm based on MERITS[1] was applied to reconstruct normalized images of the breast phantom.**The model, however, does not distinguish between different layers such as glandular tissue, and it uses an average dielectric property for the entire phantom shown in 4.4.**

In the simulation, the dielectric properties were set to $\varepsilon_r = 30.28$ and $\sigma = 2.02067$ S/m, which represent the average values for the various tissue layers. These values were intentionally chosen to make tumor detection more challenging by closely matching the properties of the tumor and the surrounding tissue, thus reducing the contrast between them.

The simulation setups with tumor and the corresponding 2D and 3D images generated using the DAS algorithm in Matlab with the help of Microwave Radar-based Imaging (MERITS)[1] are shown below:

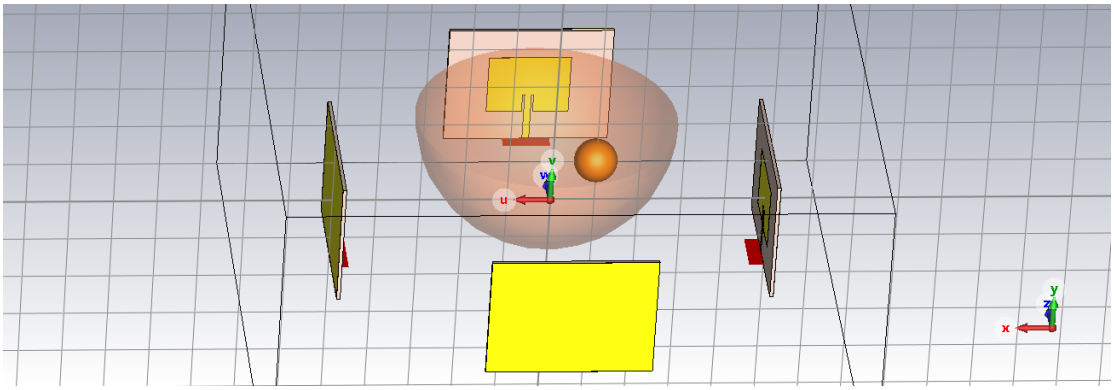

Figure 4.6: Simulation setup at location 1 offset from center.

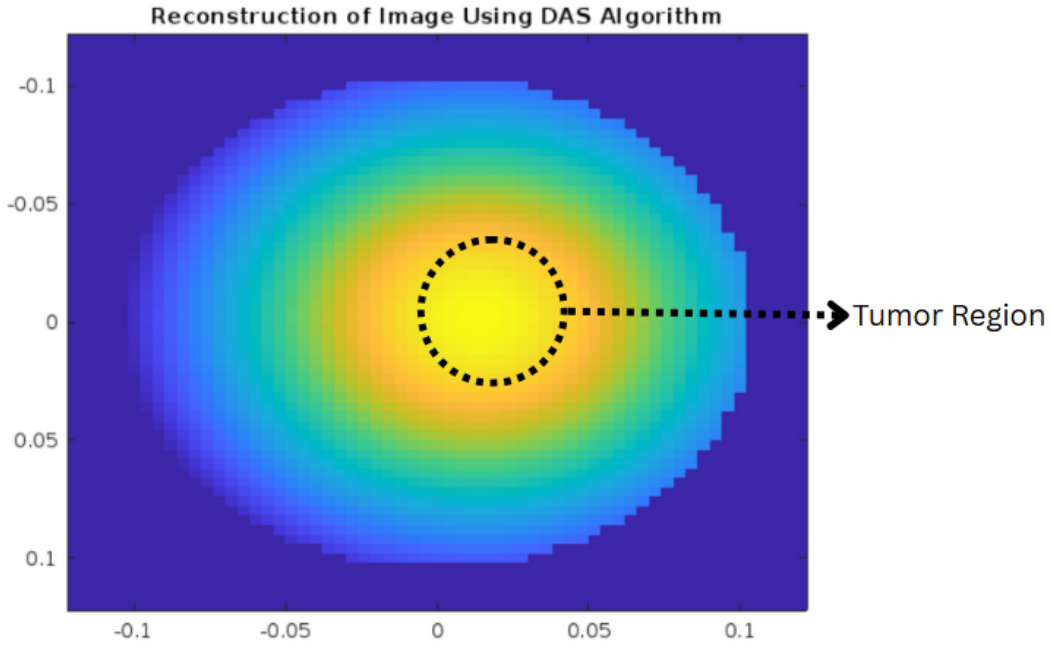

Figure 4.7: 2D image generated using DAS algorithm at location 1 in matlab.

In this study, the imaging domain is defined as a 3D grid of points over the breast phantom to evaluate the performance of the Delay and Sum (DAS) algorithm. The phantom has dimensions of 120 mm along each axis, and the image domain is discretized into 140,274 points. The grid points represent the coordinates in 3D space where the image is reconstructed.

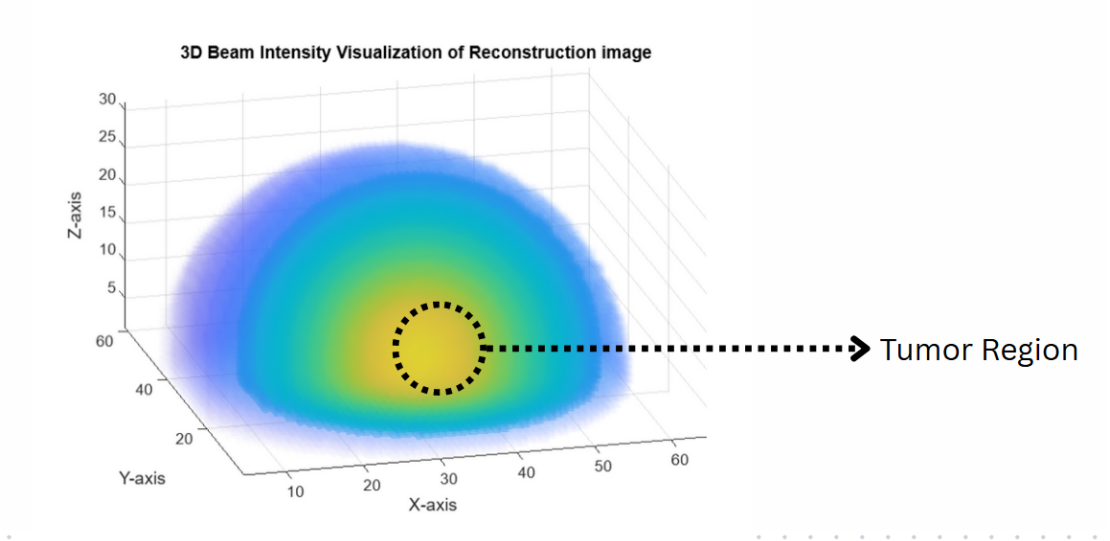

Figure 4.8: 3D image Reconstructed using DAS algorithm at tumor offset from center in matlab.

4.7.4 Image Domain for Two Antennas

To evaluate the performance of the DAS algorithm on two antenna. The imaging domain was divided into **219,488 coordinate points**, and the DAS algorithm based on MERITS [1] was applied to reconstruct normalized images of the breast phantom. For the two-antenna setup, with the phantom of size 120 mm placed between the antennas. The reconstructed 2D and 3D images of the breast phantom with a tumor with help of Microwave Radar-based Imaging(MERITS) [1] are shown below.

The image domain is discretized into a 3D grid with the following dimensions:

- **Antenna 1 :** is located at the origin: $(0,0,0)$ mm.
- **Antenna 2 :** is located at $(194.93,0,0)$ mm.

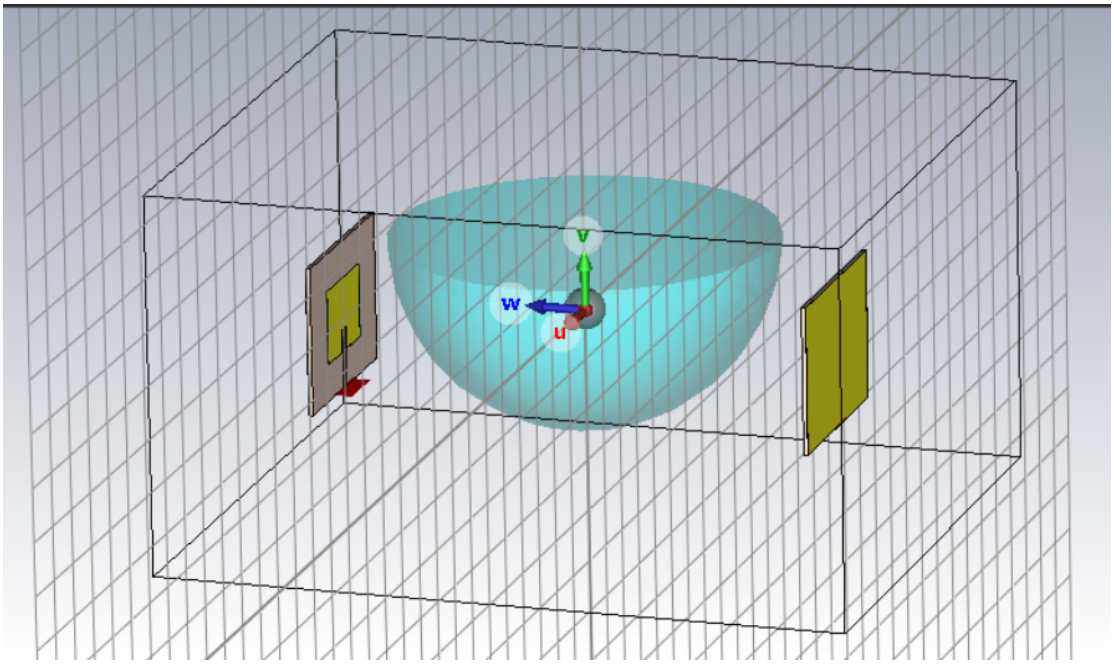

Figure 4.9: Simulation setup for two antennas with the phantom placed between them.

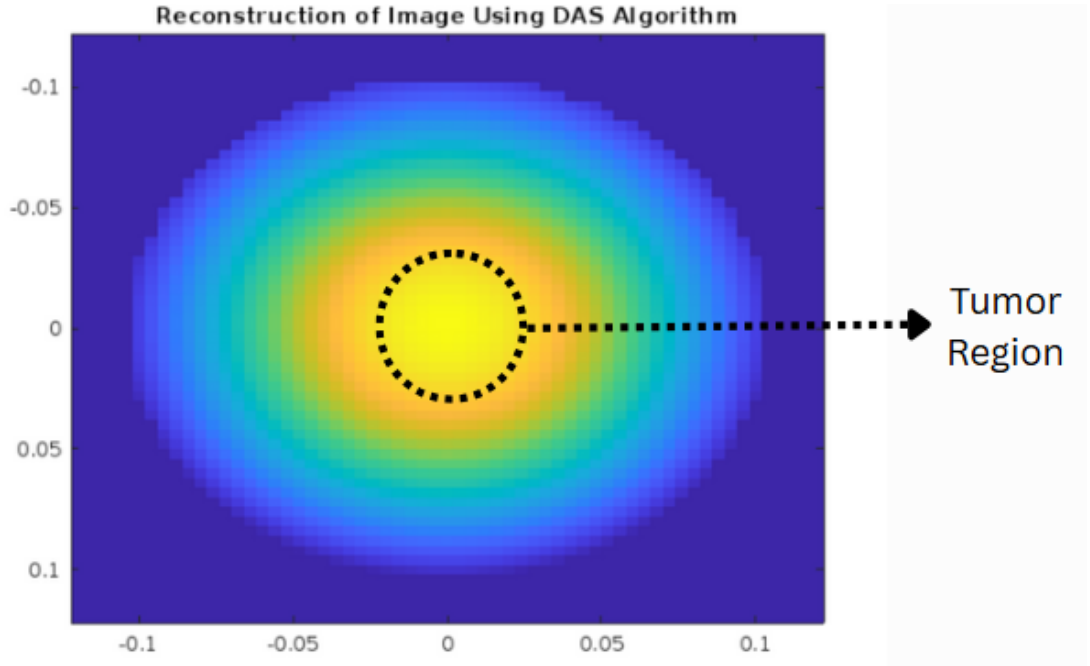

Figure 4.10: 2D image generated using DAS algorithm at tumor at center in matlab

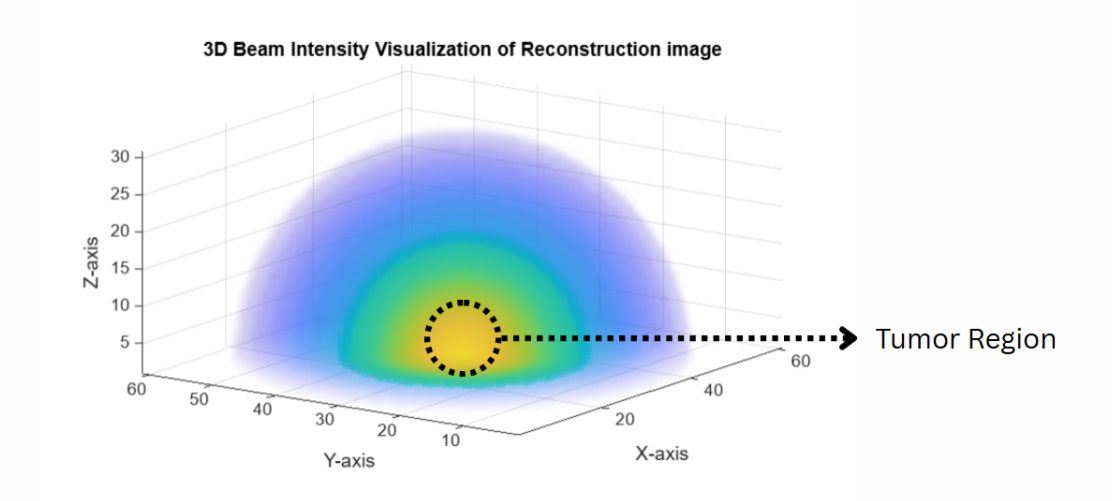

Figure 4.11: 3D image Reconstructed using DAS algorithm at tumor at center in matlab.

4.8 Experimental Setup

Since, we do not have access to a Vector Network Analyzer (VNA) capable of efficiently exciting multiple antennas simultaneously, we have optimized our experimental setup using the available resources. A Nano VNA is employed, which is limited to exciting only two antennas at a time. Consequently, the experimental setup is designed with two antenna positions located at coordinates (0, 0, 0) and (200, 0, 0) in mm. These positions are strategically chosen to ensure optimal coverage of the imaging domain.

For the imaging domain, a phantom with a radius of 40 mm is used to simulate the human breast. The phantom contains a tumor filled with normal water, which has a dielectric constant of approximately 78. This value is comparable to the dielectric properties of a tumor, ensuring a realistic signal interaction within the phantom. The experiment aims to generate and analyze the resulting data to reconstruct a 2D image of the tumor using the algorithms implemented.

The phantom, representing the imaging domain, is created with two main components: an outer layer mimicking the dielectric properties of breast tissue (as dielectric constant of ABS at 2.45 GHz is typically in the range of 2.2 to 2.6) and a tumor positioned inside the phantom, filled with normal water to achieve a high dielectric contrast relative to the surrounding medium. The tumor is intentionally designed to be irregular in shape to simulate a more realistic tumor model. Both the phantom and the tumor are 3D-printed for precision and to ensure consistency in their structure.

Phantom and Tumor

The phantom is 3D-printed with a radius of 40 mm to simulate the human breast. The irregularly shaped tumor is also 3D printed and placed inside the phantom, filled with normal water. Although the phantom does not precisely replicate the dielectric properties of human breast tissue, the dielectric contrast between the tumor and the surrounding material is intentionally enhanced. This difference in dielectric properties ensures that the tumor can be effectively distinguished and reconstructed in the final image.

Figure 4.12: 3D print of the phantom.

Figure 4.13: 3D print of the tumor.

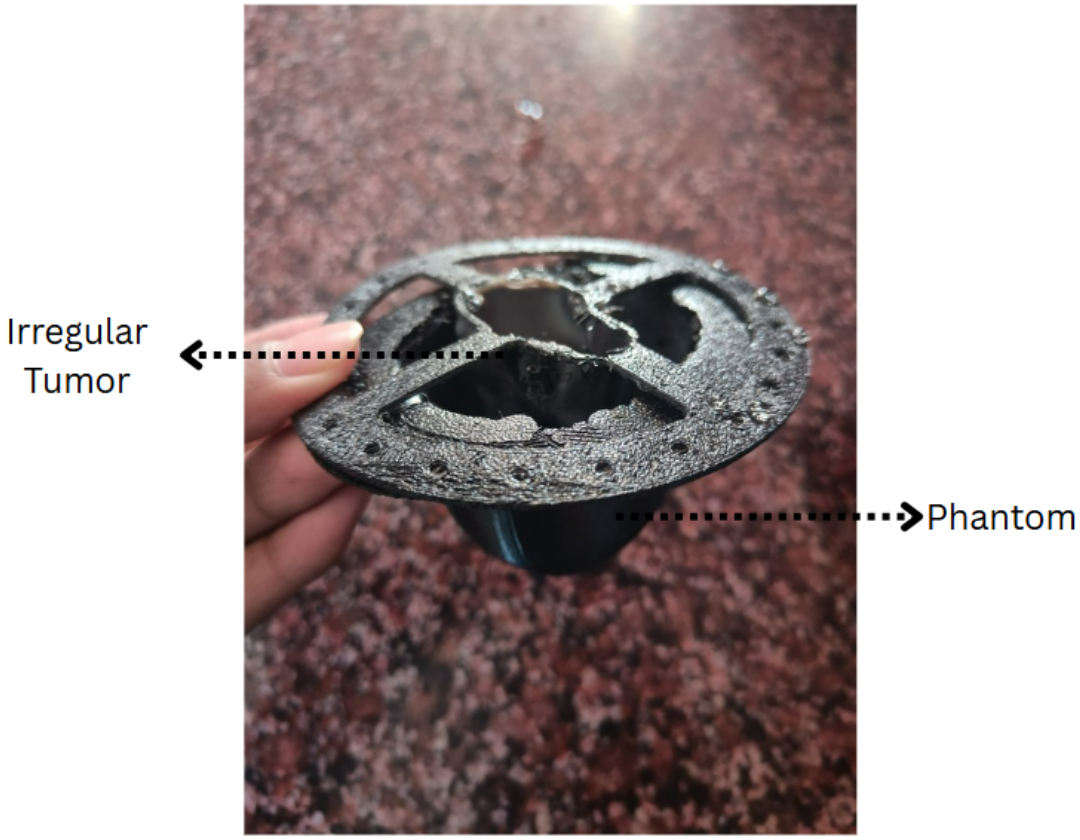

Figure 4.14: 3D printout of the phantom with the irregular tumor inside.

The tumor is filled with normal water, which has a high dielectric constant, to simulate the properties of a human tumor for better signal interaction and imaging.

4.8.1 Initial Setup and Antenna Configuration

The antennas are placed at coordinates (0, 0, 0) and (200, 0, 0) in mm, with the Nano VNA used for data acquisition. The setup is designed to excite the antennas and gather reflection signal and alternately, recording scattering data from the second antenna as it receives the transmitted signal from the first antenna. This process is repeated with the antennas switching roles to gather sufficient data for the reconstruction algorithms.

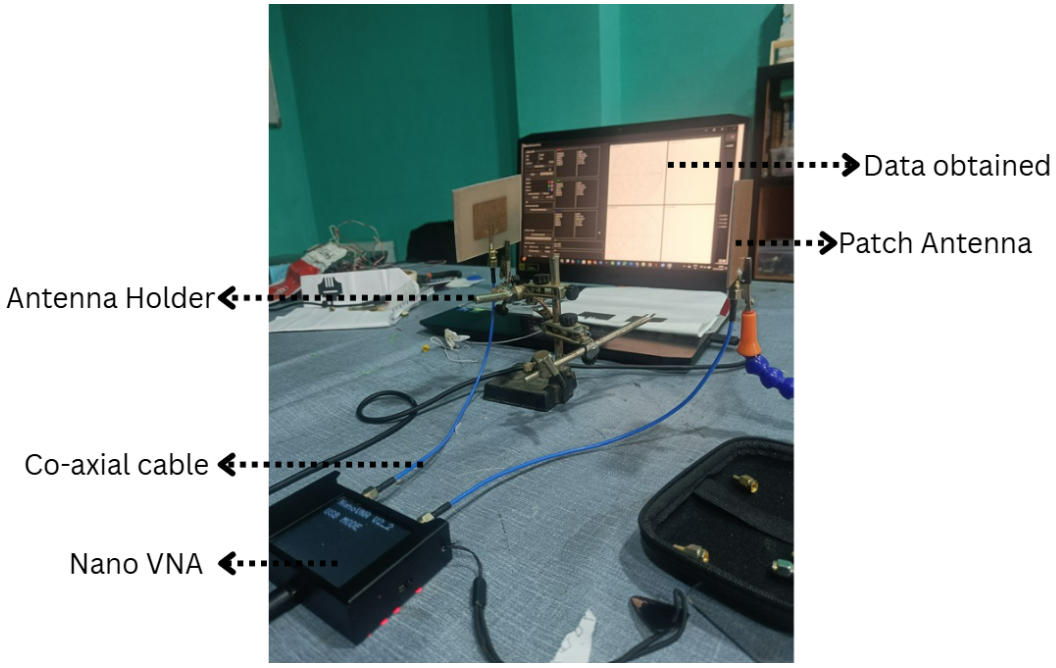

Figure 4.15: Schematic of the experimental setup, showing the antenna placement at coordinates (0, 0, 0) and (200, 0, 0) in mm, and the Nano VNA connected to the antennas for data acquisition.

4.8.2 Reconstructed 2D Image at initial setup

After collecting the scattering data from the antennas along with signal processing and Inverse Chirp Z-transform then the DAS algorithms was used to reconstruct a 2D image of the phantom. The image generated highlights regions of high dielectric contrast, which correspond to the tumor within the phantom. This 2D image is an essential step in validating the effectiveness of the experimental setup and the algorithms used for image reconstruction.

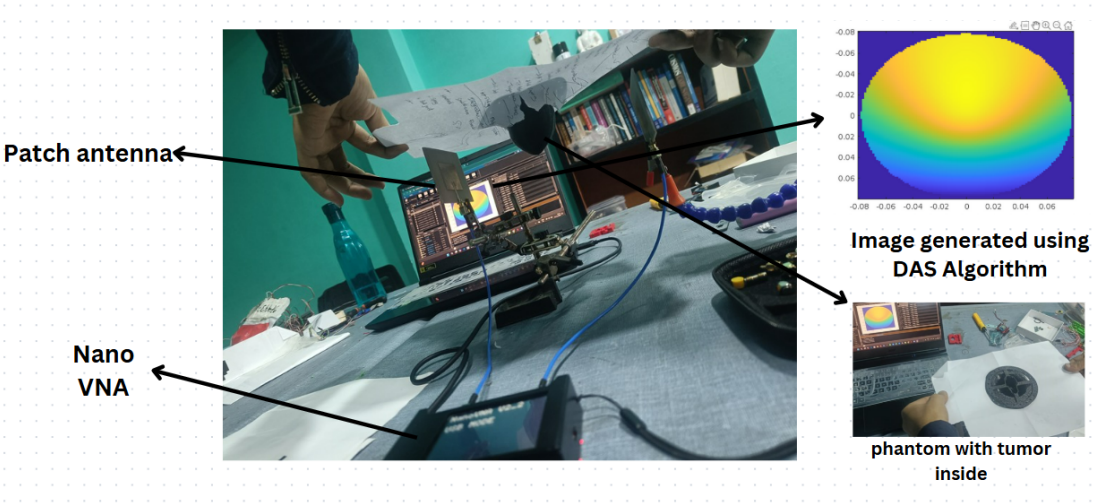

Figure 4.16: Reconstructed image from the DAS algorithms, showing tumor localization within the phantom. The image, presented in its non-normalized form, highlights the tumor's present high dielectric contrast.

4.9 Setup Design in SolidWorks

Initially, an eight-antenna setup was designed in SolidWorks for the experimental setup. However, due to the availability of a Nano VNA, which can only excite two antennas at a time, a secondary design was created with a two-antenna holder. The final experimental setup employs a Nano VNA, with two antennas positioned at coordinates $(0,0,0)$ mm and $(200,0,0)$ mm. These positions were strategically selected to ensure optimal coverage of the imaging domain. Figures 4.17 and 4.18 illustrate the initial eight-antenna design and the final two-antenna setup, respectively.

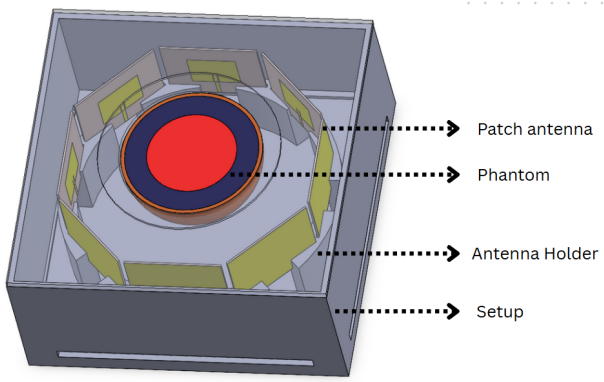

Figure 4.17: SolidWorks design of the initial eight-antenna setup.

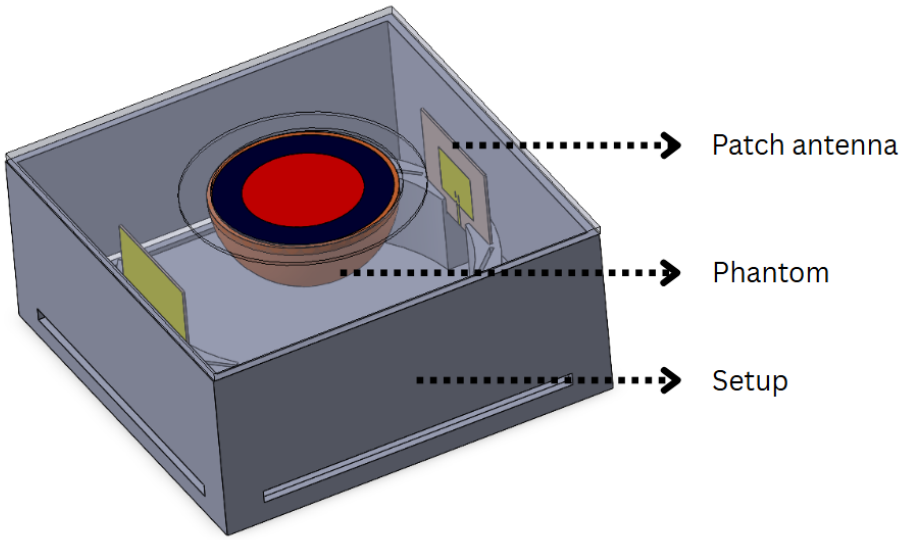

Figure 4.18: SolidWorks design of two-antenna setup due to Nano VNA limitations.

4.9.1 Final two antenna Setup and Data Acquisition

The antennas are positioned at (0,0,0) mm and (100,0,0) mm, inside a fully enclosed glass system. The NanoVNA 0.6.2 software is used for data acquisition. One antenna transmits a signal while the other receives it, capturing both reflection and scattering data.

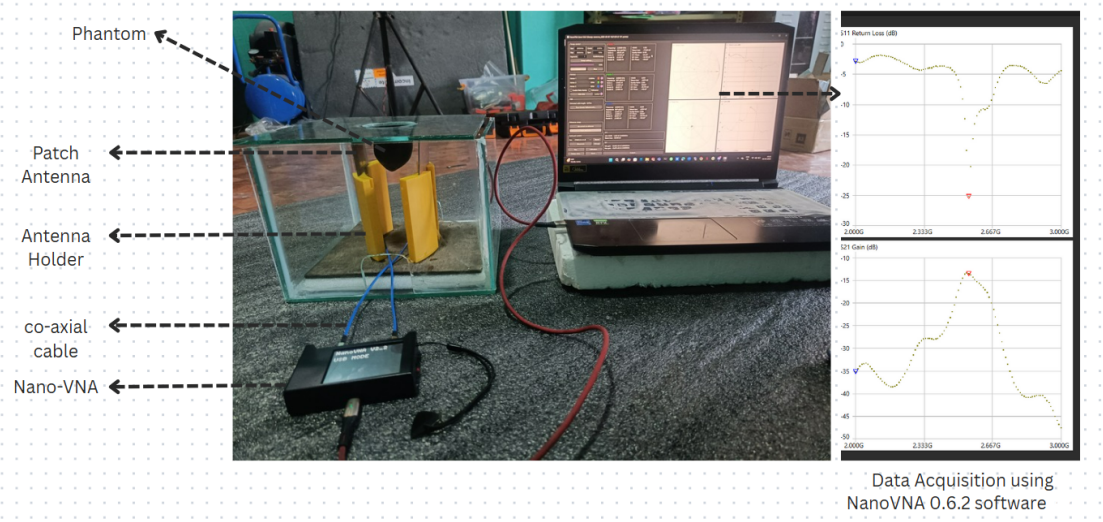

Figure 4.19: Schematic of the experimental setup, showing antennas at (0,0,0) mm and (100,0,0) mm, with the NanoVNA connected for data collection inside a fully enclosed glass system.

4.9.2 Reconstructed 2D Image at Final setup

After collecting the scattering data from the antennas, the signal undergoes processing, starting with artifact removal to eliminate noise. Tumor localization is achieved by subtracting signals with and without the tumor. The processed data is then transformed using the Inverse Chirp Z-transform before applying the DAS algorithm to reconstruct a 2D image of the phantom. This image highlights areas of high dielectric contrast, indicating the tumor's presence.

Marble was used as a tumor substitute in our experiment setup, placed in water. While it doesn't replicate the exact dielectric properties of real tumor tissue, it provides a reasonable contrast for initial testing and calibration.

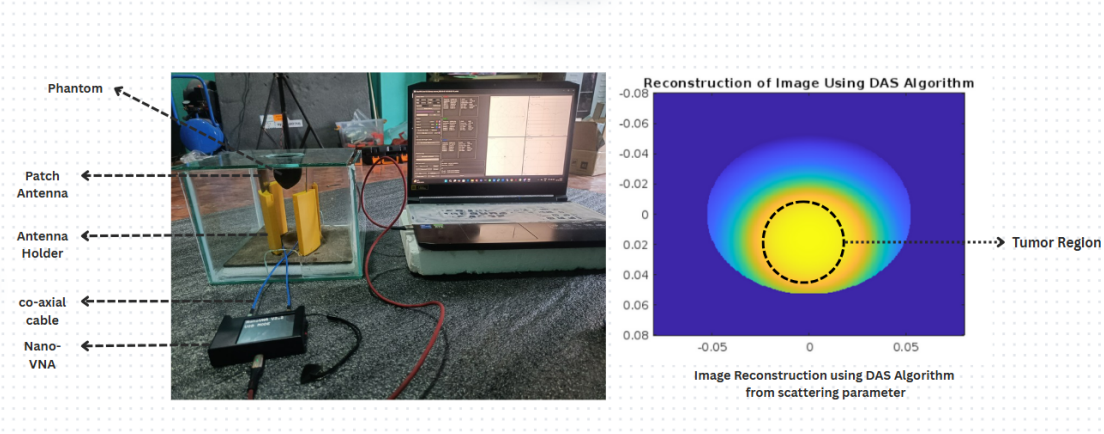

Figure 4.20: 2D image of the phantom with the tumor at the center, highlighting high dielectric contrast.

4.9.3 Plausable reasons for deviation in result of simulated and experiment

- The marble has a dielectric constant (5-10) that is very less than water (approx 78). It will be beneficial to use object that has high dielectric than water as tumor for better result.
- Use of only two antennas could not capture most part of the phantom and the signal. It will be more benefical to use higher number of antennas and multi-port vna (may be 4 or 6 or 8 or 16).
- The vna used was not of high quality as the s-parameters were fluctuating. It will be beneficial if high quality vna is used.
- The current Delay-and-Sum (DAS) algorithm may not provide optimal accuracy. Therefore, exploring alternative algorithms such as Delay-Multiply-and-Sum (DMAS) and Coherence Delay-and-Sum (CDAS) could yield better results.

4.10 Problems Faced

4.10.1 Unavailability of Vector Network Analyzer (VNA)

The primary limitation faced during the project was the unavailability of a functioning Vector Network Analyzer (VNA). Although a VNA is present in our college laboratory, it is not in working condition. Furthermore, no alternative VNA is available within the valley, creating a significant hurdle for the operation and testing of multiple antennas.

4.10.2 Limited and Incomplete Documentation

The documentation available for this project is highly limited and mostly incomplete. Since this area is still in the research phase, there has been no robust work conducted. Resources, open-source data, and algorithms are limited, making it difficult to establish a strong foundation for development.

Also, Debugging the already developed algorithms proved to be challenging due to limited resources and insufficient documentation. The lack of detailed guidelines and proper documentation created significant obstacles in identifying and resolving issues in the algorithms.

4.10.3 Unavailability of Anechoic Chamber

Another limitation is the unavailability of an anechoic chamber, which is an isolated room free from electromagnetic signals, essential for accurate antenna testing. The absence of such a facility has constrained the ability to validate the performance of the antenna system effectively.

4.11 Budget Analysis

The budget analysis for the project outlines material and production costs. The materials, including substrates, copper plates, wires, plastic shells, and glass setups, amounted to approximately NRs. 5565. Production expenses, such as manufacturing, documentation, and miscellaneous costs, added up to NRs. 6000, bringing the total estimated budget to NRs. 11,565. The analysis highlights the affordability of the system, reinforcing its potential as a cost-effective solution for breast cancer detection in resource-limited settings.

4.12 Work Schedule

The project began with a literature review from May 20th to February 20th, during which we gathered essential information to guide the approach. Following this, the project proposal was completed from June 1st to June 6th, outlining our objectives and

S.N	Material Cost	Estimation(in NRs.)
1	Substrate	3300
2	Copper Plate	565
3	Copper Wire	200
4	Plastic Shell and phantom	500
5	Glass setup	1000
5	Total	5565

Table 4.1: Material Cost Estimation

S.N	Description	Estimation(in NRs.)
1	Manufacturing Cost	2000
2	Documentation	3000
3	Miscellaneous	2000
4	Total Cost	6000

Table 4.2: Production Cost Estimation

methodology. The design and simulation of the patch antenna took place between June 1st and July 30th, with results analyzed from August 1st to September 15th. During this period, we also collected the necessary components, including the SMA connector, laminated PCB, 50-ohm coaxial cable, etching chemicals, and other supplies for antenna fabrication.

The antenna was fabricated from September 24th to October 13th, and the phantom model for testing was created from October 14th to 18th. The microwave imaging phase started on October 14th and continued until February 15th, during which we tested the antenna system on the phantom model, analyzed the data, and implemented DAS algorithms. The experimentation phase began on December 1st and continued until February 18th, during which we focused on evaluating the system's performance. Finally, the documentation phase took place from November 30th to March 1st, where we wrote the detailed report summarizing the entire project.

The following table shows the tasks, their starting date , and the end date .

S.N.	**Task**	**Start Date**	**End Date**
1	Literature Review	20 May	20 Feb
2	Proposal	1 June	6 June
3	Patch Antenna Design and Simulation	1 June	30 July
4	Simulation Result Interpretation	1 August	15 Sept

S.N.	Task	Start Date	End Date
5	Material Collection	16 Sept	23 Sept
6	Antenna Fabrication	24 Sept	13 Oct
7	Phantom Design and Fabrication	14 Oct	18 Oct
8	Microwave Imaging	16 Oct	15 Feb
9	Source Design and Fabrication	1 Nov	30 Jan
10	Experimentation Setup Design	1 Nov	15 Jan
11	Experimentation	1 Dec	1 March
12	Documentation	30 Nov	4 March

Table 4.3: Project Tasks, Start and End Dates

A Gantt chart will provide a visual representation of our project timeline, ensuring that each task stays on track and is completed within the planned timeframe.

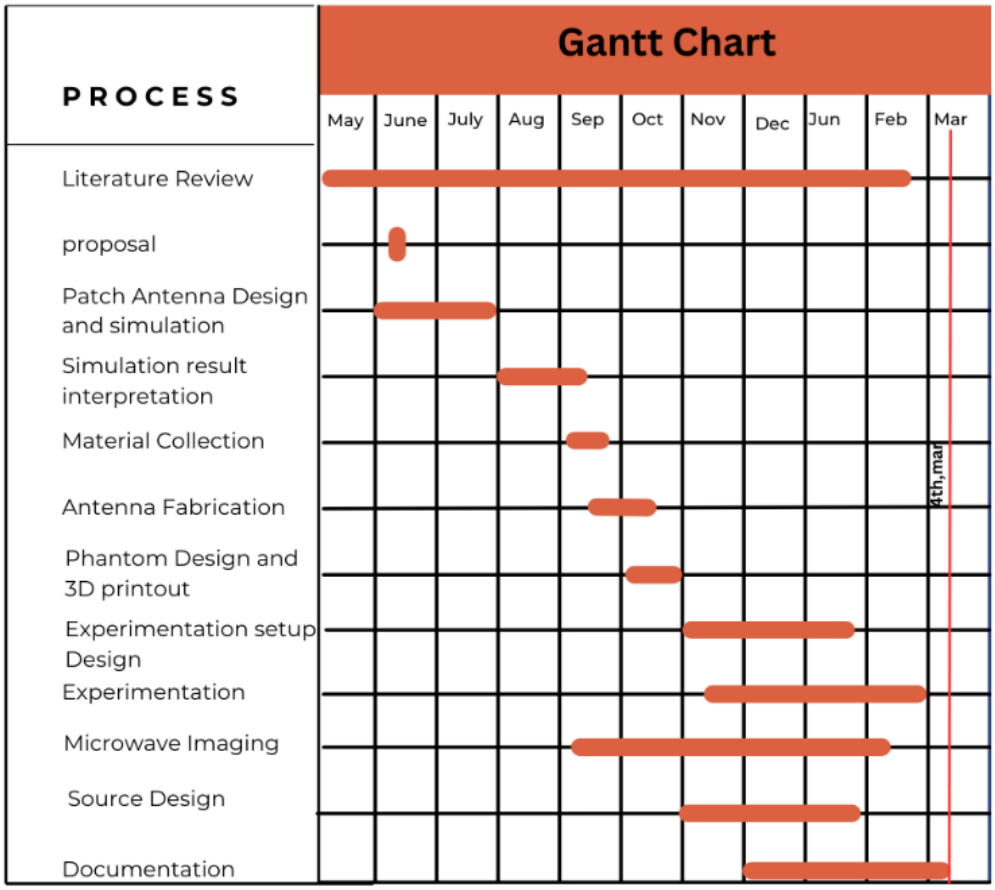

Figure 4.21: Gantt Chart of Project Timeline

CHAPTER 5:
CONCLUSION AND FUTURE ENHANCEMENT

This study aimed to develop a non-invasive, cost-effective microwave imaging system using microstrip patch antennas for early breast cancer detection. The project successfully demonstrated the feasibility of this approach through simulation, achieving promising results in tumor identification and imaging for simplistic breast phantom. However, discrepancies arose between simulation and experimental outcomes, highlighting critical challenges that require further investigation.

5.1 Key Achievements

5.1.1 Antenna Design and Optimization

- Successfully designed a microstrip patch antenna in CST Microwave Studio to resonate at 2.404 GHz, suitable for microwave imaging applications.
- The antenna was optimized for impedance matching, return loss, and bandwidth performance to ensure efficient energy transmission and reception in a biomedical setup.

5.1.2 Antenna Fabrication and Validation

- The designed antenna was fabricated using an FR4 substrate through etching PCB with Ferric Chloride (FeCl3) called photo-lithography technique.
- Experimental testing using a two-port NanoVNA confirmed a resonance frequency obtained at 2.5GHZ , validating the accuracy of the CST design and confirming functional performance.

5.1.3 Simulation-Based Image Reconstruction

- Developed and implemented the Delay-and-Sum (DAS) algorithm in MATLAB for image reconstruction using simulated S-parameters.
- Achieved successful reconstruction of 2D and 3D tumor images in simulation, demonstrating high localization accuracy and validating the theoretical imaging

framework.

5.1.4 Experimental Validation Using Phantom Model

- Created a 3D-printed breast phantom with an irregular-shaped tumor substitute (marble or water-filled) to mimic realistic tissue conditions.
- Preliminary experimental data was collected using the fabricated antennas and processed through the DAS algorithm. While the reconstructed images were less distinct than in simulation, they provided a practical basis for system validation and further enhancement.

5.2 Challenges and Limitations

The experimental phase faced significant hurdles:

- **Hardware Constraints:** The limited two-port NanoVNA restricted the system to only two antennas, reducing data resolution and coverage. Commercial VNAs with multi-port capabilities are essential for robust signal acquisition.
- **Low-Power VNA:** The NanoVNA's limited power output (compared to clinical-grade systems) resulted in weak signal penetration and poor signal-to-noise ratios, affecting tumor detection.
- **Phantom Limitations:** Substituting tumors with cork/marble introduced inaccuracies, as these materials lack the dielectric properties (e.g., $\varepsilon_r \approx 50$, $\sigma \approx 4$ S/m) of real malignant tissues.
- **Environmental Noise:** The absence of an anechoic chamber led to electromagnetic interference, further degrading experimental data quality.

5.3 Future Directions

To bridge the gap between simulation and real-world application, the following enhancements are proposed:

1. **Multi-Antenna Array:** Implement a 16-antenna setup with a multi-port VNA to improve spatial resolution and signal diversity.

2. **Biomimetic Phantoms:** Develop phantoms using agar, saline, and polyethylene glycol to replicate human tissue dielectric properties accurately.

3. **Advanced Hardware:** Use high-power VNAs and integrate amplifiers to enhance signal penetration and dynamic range.

4. **Algorithm Optimization:** Refine the DAS algorithm with artifact-removal techniques (e.g., adaptive filtering) and explore machine learning models for noise reduction.

5.4 Significance

Despite experimental limitations, this work lays a foundation for microwave-based breast cancer detection as a safer alternative to ionizing radiation methods. The system's low cost, portability, and non-invasive nature align with global healthcare needs, particularly in resource-limited settings. Future iterations addressing hardware and phantom constraints could revolutionize early diagnosis, reducing mortality rates through timely intervention.

5.5 Final Statement

This project underscores the potential of microwave imaging while emphasizing the importance of interdisciplinary collaboration between engineering and medical fields to translate theoretical models into clinical tools. By addressing current limitations, this technology could one day complement or even replace conventional methods, offering a radiation-free pathway to saving lives.

CHAPTER 6:
ANNEXURE

Frequency to Time Domain Conversion based on Merits[1]

```
% ===== Frequency to Time Domain Conversion =====
% Uses Chirp Z-Transform (CZT) for efficient computation

function [signals2d] = fd2td(signals, frequencyAxis, timeAxis)

validateattributes(signals, {'numeric'},
{'nrows', numel(frequencyAxis)});

validateattributes(frequencyAxis, {'numeric'},
{'vector', 'increasing', 'real'});

validateattributes(timeAxis, {'numeric'},
{'vector', 'increasing', 'real'});

if diff(timeAxis(1:2)) * numel(timeAxis)
 \textgreater range(timeAxis)

error('Time axis needs to be linearly sampled');

end

if diff(frequencyAxis(1:2)) * numel(frequencyAxis)
\textgreater range(frequencyAxis)

error('Frequency axis needs to be linearly sampled');

end

signals2d = reshape2d(@fd2tdInternal, signals);

function [signals2d] = fd2tdInternal(signals)

timeAxis = timeAxis(timeAxis \textgreater 0);

dt = diff(timeAxis(1:2));

df = diff(frequencyAxis(1:2));

m = numel(timeAxis);

w = exp(-1j * 2 * pi * dt * df);
```

```
a = exp(1j * 2 * pi * min(timeAxis(:)) * df);

iczt = @(z) conj(czt(conj(z), m, w, a));

phase = exp(1j * 2 * pi * min(frequencyAxis(:))
.* timeAxis(:));

phaseCompensation = @(z) real(phase(:) .* z) / m;

signals2d = phaseCompensation(iczt(signals));

end

end
```

Delay Calculation

```
% ===== Delay Calculation =====
% Introduces delays to signals based on specified parameters

function [signals2d] = delay(signals,
delays, axisParam, paddingFunc)

if \textgreater exist('paddingFunc', 'var')

paddingFunc = @nan;

end

if isreal(signals)

if nargin == 2

validateattributes(delays, {'numeric'}, {'integer'});

signals2d = reshape2d(@delaySample, signals, delays);

elseif nargin \textgreater 3 &&
numel(axisParam) == size(signals, 1)

validateattributes(axisParam, {'numeric'},
 {'vector', 'increasing', 'real'});

if diff(axisParam(1:2)) * numel(axisParam)
\textgreater range(axisParam)

error('Time axis needs to be linearly sampled');
```

```
end

dt = diff(axisParam(1:2));

signals2d = reshape2d(@delaySample, signals,
round(delays ./ dt));

elseif nargin == 3 && isa(axisParam, 'function_handle')

paddingFunc = axisParam;

validateattributes(delays, {'numeric'}, {'integer'});

signals2d = reshape2d(@delaySample, signals, delays);

end

elseif \textgreaterisreal(signals) && nargin == 3

signals2d = signals .* exp(-2i * pi
* (delays .* axisParam(:)));

else

signals2d = signals;

end

function [signals2d] = delaySample(signals, delays)

signals2d = paddingFunc(size(signals), 'like', signals);

signals2d(:, delays == 0) = signals(:, delays == 0);

for d = unique(delays(:))'

cs = delays == d;

\texttt{if d \textgreater 0}

signals2d(d + 1:end, cs) = signals(1:end - d, cs);

\texttt{else}

signals2d(1:end + d, cs) = signals(1 - d:end, cs);

\texttt{end}
```

```
end

end

end
```

Delay Computation for Channels

```
% ===== Delay Computation for Channels =====
% Computes and applies delays for each channel in the
received signals

function [delayedSignals] = computeDelayForChannels
(signals, delays)

numChannels = size(signals, 2);

delayedSignals = zeros(size(signals));

for ch = 1:numChannels

delayedSignals(:, ch) = delay(signals(:, ch), delays(ch), []);

end

end
```

Signal Processing for Image Reconstruction

```
% ===== Signal Processing for Image Reconstruction =====
% Processes the delayed signals for image reconstruction using
DAS and DMAS algorithms

function [reconstructedImage] = reconstructImage(signals, delays)

delayedSignals = computeDelayForChannels(signals, delays);

% Apply DAS (Delay and Sum) algorithm

reconstructedImage = sum(delayedSignals, 2);

end
```

Final Image Slice Extraction

```
% ===== Final Image Slice Extraction =====
% Extracts the image slice from the reconstructed image
```

```
delays = getDelays(channelNames, antennaLocations,
relativePermittivity);

imSlice = getSlice(img, points, axisParam);

figure();

imshow(imSlice, []);

title('Constructed Image');
```

BIBLIOGRAPHY

[1] D. O'Loughlin, A. Elahi, E. Porter, A. Shahzad, B. Oliveira, M. Glavin, E. Jones, and M. O'Halloran, "Open-source software for microwave radar-based image reconstruction," 04 2018.

[2] ICNIRP, "Guidelines for Limiting Exposure to Electromagnetic Fields (100 kHz to 300 GHz)," *Health Physics*, vol. 118, pp. 483–524, May 2020.

[3] IEEE, "IEEE Standard for Safety Levels with Respect to Human Exposure to Radio Frequency Electromagnetic Fields," 2019.

[4] FCC, "OET Bulletin 65: Human Exposure to Radiofrequency Electromagnetic Fields," tech. rep., FCC, 2021.

[5] K. S. and L. S., "In-place calibration with single measurement in time-domain microwave breast imaging," 2016.

[6] I. A. for Research on Cancer, "Worldwide cancer data: World cancer research fund international," May 2024. Accessed: 6 June 2024.

[7] V. Jeyakumar, "Design and development of single layer microstrip patch antenna for breast cancer detection," *Bonfring International Journal of Research in Communication Engineering*, vol. 2, p. 14, 07 2012.

[8] J. A. Cullinan, "Mammography and beyond: Developing technologies for the early detection of breast cancer," *American Journal of Roentgenology*, vol. 179, no. 1, pp. 42–42, 2002.

[9] S. W. Fletcher and J. G. Elmore, "Mammographic screening for breast cancer," *New England Journal of Medicine*, vol. 348, no. 17, pp. 1672–1680, 2003.

[10] D. D. Adler, P. L. Carson, J. B. Rubin, and K. A. Quinn-Reid, "Doppler ultrasound color flow imaging in the study of breast cancer: preliminary findings," *Ultrasound in Medicine & Biology*, vol. 16, no. 6, pp. 553–559, 1990.

[11] *Thermal Analysis of Cancerous Breast Model*, vol. Volume 2: Biomedical and Biotechnology of *ASME International Mechanical Engineering Congress and Exposition*, 11 2012.

[12] P. M. Meaney, M. W. Fanning, D. Li, S. P. Poplack, and K. D. Paulsen, "A clinical prototype for active microwave imaging of the breast," *IEEE Transactions on Microwave Theory and Techniques*, vol. 48, no. 11, pp. 1841–1853, 2000.

[13] H. Health, "Radiation risk from medical imaging," 30 September 2021. Accessed: 6 June 2024.

[14] S. Medicine, "Risks of magnetic resonance imaging (mri)," May 2024. Accessed: 6 June 2024.

[15] Y. Cheng and M. Fu, "Dielectric properties for non-invasive detection of normal, benign, and malignant breast tissues using microwave theories," *Thoracic Cancer*, vol. 9, no. 4, pp. 459–465.

[16] S. C. Hagness, A. Taflove, and J. E. Bridges, "Two-dimensional fdtd analysis of a pulsed microwave confocal system for breast cancer detection: fixed-focus and antenna-array sensors," *IEEE Transactions on Biomedical Engineering*, vol. 45, no. 12, pp. 1470–1474, 1998.

[17] S. Gabriel, R. W. Lau, and C. Gabriel, "The dielectric properties of biological tissues: Ii. measurements in the frequency range 10 hz to 20 ghz," *Physics in Medicine and Biology*, vol. 41, no. 11, pp. 2251–2269, 1996.

[18] M. Solis-Nepote, T. Reimer, and S. Pistorius, "An air-operated bistatic system for breast microwave radar imaging: pre-clinical validation," in *2019 41st Annual International Conference of the IEEE Engineering in Medicine and Biology Society (EMBC)*, pp. 1859–1862, IEEE, 2019.

[19] M. M. Rana, *Development and evaluation of a sensor and antenna array for a portable microwave-based breast cancer detection system*. PhD thesis, University of Manitoba, 2021.

[20] P. Meaney, M. Fanning, D. Li, S. Poplack, and K. Paulsen, "A clinical prototype for active microwave imaging of the breast," *IEEE Transactions on Microwave Theory and Techniques*, vol. 48, no. 11, pp. 1841–1853, 2000.

[21] E. Avsar Aydin, "A preliminary study for early breast cancer detection with microwaves," *Tehnički glasnik*, vol. 12, no. 2, pp. 109–112, 2018.

[22] S. M. Chouiti, L. Merad, S. M. Meriah, X. Raimundo, and A. Taleb-Ahmed, "An efficient image reconstruction method for breast cancer detection using an ultra-wideband microwave imaging system," *Electromagnetics*, vol. 36, no. 4, pp. 225–235, 2016.

[23] A. Aydin and E. Avsar Aydin, "Evaluation of limestone layer's effect for uwb microwave imaging of breast models using neural network," *Tehnički glasnik*, vol. 11, no. 1-2, pp. 50–54, 2017.

[24] A. F. Yahya, Y. M. Abbosh, and A. Abbosh, "Microwave imaging method employing wavelet transform and neural networks for breast cancer detection," in *Asia-Pacific Microwave Conference 2011*, pp. 1418–1421, IEEE, 2011.

[25] X. Wang, D. R. Bauer, R. Witte, and H. Xin, "Microwave-induced thermoacoustic imaging model for potential breast cancer detection," *IEEE Transactions on Biomedical Engineering*, vol. 59, no. 10, pp. 2782–2791, 2012.

[26] R. Díaz-Uriarte and S. A. de Andrés, "Gene selection and classification of microarray data using random forest," *BMC Bioinformatics*, vol. 7, pp. 3 – 3, 2006.

[27] L. Vibha, G. Harshavardhan, K. Pranaw, P. Shenoy, K. Venugopal, and L. Patnaik, "Statistical classification of mammograms using random forest classifier."

[28] P. E., S. A., C. M., and P. M., "An experimental system for time-domain microwave breast imaging," in *Proceedings of the 5th European Conference on Antennas and Propagation (EUCAP '11)*, (Rome, Italy), pp. 11–15, April 2011.

[29] K. M., C. I. J., L. J. A., P. A., and B. R., "Radar-based breast cancer detection using a hemispherical antenna array—experimental results," *IEEE Transactions on Antennas and Propagation*, vol. 57, no. 6, pp. 1692–1704, 2009.

[30] S. W., Z. B., Z. Z., and W. G., "Uwb microwave imaging for breast tumor detection in inhomogeneous tissue," in *Proceedings of the 27th Annual International Conference on Engineering in Medicine and Biology Society (EMBS '05)*, (Shanghai, China), pp. 1496–1499, 2005.

[31] A. et al., "Microwave radar-based image reconstruction," 2017. Accessed: 2024-12-15.

[32] https://www.facebook.com/verywell, "Breast Anatomy Is Complex and Intricate — verywellhealth.com." `https://www.verywellhealth.com/parts-of-a-nipple-and-areola-430642`. [Accessed 15-12-2024].

[33] Rajiv, "Vector Network Analyzer Basics - RF Page — rfpage.com." `https://www.rfpage.com/vector-network-analyzer-basics/`. [Accessed 15-12-2024].

[34] "Vector Network Analyzer tutorial — VNA tutorial — rfwireless-world.com." `https://www.rfwireless-world.com/Tutorials/Vector-Network-Analyzer-VNA-tutorial.html`. [Accessed 15-12-2024].

[35] E. C. Fear and M. A. Stuchly, "Microwave detection of breast cancer," *IEEE Transactions on Microwave Theory and Techniques*, vol. 48, pp. 1854–1863, Nov. 2000.